JBIC Journal of Biological Inorganic Chemistry (2021) 26:435–453
https://doi.org/10.1007/s00775-021-01865-9

ORIGINAL PAPER

Functionalized azobenzene platinum(II) complexes as putative anticancer compounds

Katia G. Samper[1] · Julia Lorenzo[2] · Mercè Capdevila[1] · Òscar Palacios[1] · Pau Bayón[1]

Received: 4 February 2021 / Accepted: 20 March 2021 / Published online: 1 May 2021

Abstract

The synthesis and characterization of four platinum(II) complexes using azobenzenes conveniently functionalized as ligands has been carried out. The characteristic photochemical behavior of the complexes due to the presence of azobenzene-type ligands and the role of the ligands in the activation of the complexes has been studied. Their promising cytotoxicity observed in HeLa cells prompted us to study the mechanism of action of these complexes as cytostatic agents. The interaction of the compounds with DNA, studied by circular dichroism, revealed a differential activity of the Pt(II) complexes upon irradiation. The intercalation abilities of the complexes as well as their reactivity with common proteins present in the blood stream allows to confirm some of the compounds obtained as good anticancer candidates.

Keywords Platinum complex · Azobenzene · Cisplatin resistance · Antitumor drug

Introduction

According to World Health Organization (WHO), cancer is, in the twenty-first century, the first or second leading cause of death before age of 70 in 91 out of 172 countries [1]. It also ranks it as the third or fourth in 22 additional countries. Unfortunately, cancer incidence and mortality are rapidly increasing in the world, due to aging and population growth factors. Diagnosed cancer cases usually require treatments based on radiotherapy, chemotherapy, surgery and others, prevailing chemotherapy as one of the main strategies to treat cancer.

Cisplatin became, decades ago, one of the most outstanding advances in chemotherapy and in the fight against cancer [2]. Since then, many efforts have been devoted to the development of new metal drugs [3, 4]. Combining both parts, metal ions and ligands, provides further possibilities in drug design. The versatility of metal ions (several oxidation states, different coordination environments, etc.) as well as the many possibilities in the design and synthesis of new ligands open up an enormous number of possibilities in the pursuit of new candidates with therapeutic properties. This is especially necessary since most metal drug approaches present a whole series of drawbacks. A broad set of unwanted side effects and low selectivity remain the most important unresolved challenges [5]. Hence, new compounds and strategies are required. A number of studies on new complexes carried out in recent years have helped to progress in the understanding of the mechanisms of action of these platinum-based drugs. Thus, apart from the accepted DNA interaction for cisplatin, other mechanisms have been revealed as responsible for the action of other cytostatic agents based equally on platinum complexes [3, 6–8].

With the aim of improving selectivity and effectiveness, one of the most promising fields in this concern is the so-called phototherapy and more specifically the photoactivated chemotherapy (PACT). This approach consists of the induction of electronic and/or conformational changes in the metal complex as a response to light. In this way, the goal is to move from an inactive complex to another active species. Thus, when and where the active drug is generated can be controlled, and therefore selectivity can be improved, consequently reducing side-effects, in comparison with

✉ Òscar Palacios
oscar.palacios@uab.cat

✉ Pau Bayón
pau.bayon@uab.cat

[1] Departament de Química, Facultat de Ciències, Universitat Autònoma de Barcelona, 08193-Cerdanyola del Vallès, Barcelona, Spain

[2] Institut de Biotecnologia i Biomedicina, Departments Bioquímica i Biologia Molecular, Universitat Autònoma de Barcelona, 08193-Cerdanyola del Vallès, Barcelona, Spain

conventional chemotherapies [9, 10]. Specifically, PACT has emerged as a good alternative to the conventional Pt(II)-based therapies [11–19] and many efforts have been made in the design of pro-drugs based on Pt(IV) that lead to final Pt(II) active species [20].

Platinum-based PACT anticancer drugs can be activated through several mechanisms [12]. Among them, photoswitching seems to be a promising choice [21–24]. The effectiveness of these procedures depends on the efficiency in light absorption, as well as on the reactivity of the corresponding photoproducts formed. Some of the advantages of photoswitches are the rapidity of response and that unwanted by-products are not usually generated. Azobenzenes are molecular motifs with good photostability and with well-known properties as molecular switches. Azobenzene units can easily absorb light, provoking its isomerization from *trans* to *cis* configuration. They have been used in various applications, as therapeutic agents [25–27], in polymer chemistry, materials and nanodevices [28–30].

In this work, azobenzene-based ligands are used for the synthesis of Pt(II) complexes. In the literature, the number of examples of platinum(II) complexes bearing azobenzene ligands is scarce, even if some anticancer activity has been suggested, mainly without taking into consideration the isomerization of the ligands [31, 32]. In this work, we have synthesized and characterized a new set of Pt(II)-azobenzene complexes with the aim of determining if the photoisomerization of azobenzenes can be useful and necessary to improve the antiproliferative activity of the respective complexes. Accordingly, their photochemical activity and reactivity in front of several biomolecules have been studied.

Experimental

Characterization of the ligands and complexes synthesized

The characterizations of the ligands synthesized and the corresponding Pt(II) complexes were carried out by several techniques and methodologies.

NMR spectra were registered at the *Servei de Ressonància Magnètica* at the *Universitat Autònoma de Barcelona* (UAB) using several Bruker spectrometers: DPX250 (250 MHz), DPX360 (360 MHz), and ARX400 (400 MHz). ^{1}H and $^{13}C\{^{1}H\}$ NMR spectra were referenced using residual solvent peaks, relative to tetramethylsilane (TMS) at 0 ppm. ^{195}Pt NMR chemical shift scale is referenced relative to K_2PtCl_4 in D_2O set at—1616 ppm. All spectra have been registered at 298 K except when specified.

UV–vis spectra were acquired using an Agilent 8453 Spectrophotometer with Diode-array detector in 1-cm thick quartz cuvettes. CD measurements were performed using a JASCO spectropolarimeter (model J-715, JASCO, Groß-Umstadt, Germany) controlled with the J700 software, (JASCO, Groß-Umstadt, Germany). Samples were analyzed in 1-cm capped quartz cuvettes, and the temperature was maintained at 25 °C with a Peltier PTC-351S holder (TE Technology, Traverse City, MI, USA). Spectra were processed using the GRAMS 32 software (Thermo Fisher Scientific, Waltham, MA, USA). Elemental analyses were carried out with a Flash EA 2000 CHNS, Thermo Fisher Scientific equipment with a TCD and a MAS 200 R autosampler for solid samples by the *Servei d'Anàlisi Química* (SAQ) at the UAB. Fluorescence measurements were carried out with a Perkin Elmer LS 55 50 Hz Fluorescence Spectrometer using a 1-cm quartz cell. The data obtained were corrected for the dilution effects by means of the OriginPro8 SR7 software (OriginLab Corporation, Northampton, MA, USA). Photoisomerization studies were carried out with continuous irradiation using a 6-W UVP UVGL-55 handheld UV lamp at 254 nm and 365 nm. High-resolution mass spectra (HRMS) were obtained with a Micro Tof-Q Instrument (Brucker Daltonics GmbH, Bremen, Germany) mass spectrometer working in high-resolution mode at *SAQ* at the UAB.

Synthesis

All commercially available reagents and solvents were used as received. Reactions were carried out under normal atmospheric conditions with no efforts to exclude moisture or oxygen, unless it is indicated. The compounds *tert*-butyl (3-bromopropyl)carbamate (**2**), *tert*-butyl (3-(4-nitrophenoxy)propyl)carbamate (**3**), *tert*-butyl (3-(4-aminophenoxy) propyl)carbamate (**4**), (*E*)-4,4′-(diazene-1,2-diyl)diphenol (**10**), (*E*)-4,4′-di(bromopropanoxy)azobenzene (**11**) were synthetized as previously described from commercially available reagents [33–36]. Complex [Pt(dmba)(dmso)Cl], **17** was synthesized according to earlier reported [37].

Synthesis of tert-butyl (E)-(3-(4-((4-hydroxyphenyl) diazenyl)phenoxy)propyl) carbamate, *5*

An adaption of the synthesis described [38] was followed. To a solution of **4** (113 mg, 0.42 mmol) in 20 mL of distilled water, 42 µL of 32% hydrochloric acid (0.42 mmol, 1 equiv) were added and the resulting solution was cooled below 5 ºC. An also cooled below 5 ºC solution of sodium nitrite (30 mg, 0.42 mmol) in 20 mL of distilled water was added dropwise to the previous cooled solution and stirred for 90 min at a temperature lower than 5 ºC. The resulting mixture was added dropwise to a cooled solution of phenol (40 mg, 0.42 mmol), sodium hydroxide (17 mg, 0.42 mmol) and sodium carbonate (47 mg, 0.44 mmol) in 50 mL of distilled water. After allowing stirring for 2 h at a temperature

lower than 10 ºC, the solution was neutralized using 32% of hydrochloric acid. The brown light solid was filtered and recrystallized in a mixed solvent of ethanol and water (1:1, v/v) to give **5** as a yellow/light-brown solid. (80 mg, 51%). ^{1}H NMR (250 MHz, $CDCl_3$): δ 7.97–7.79 (m, 4H), 6.99–6.92 (m, 4H), 4.77 (br, 1H), 4.07 (t, 2H, *J* = 5.9 Hz), 3.36 (q, 2H, *J* = 6.7 Hz, *J* = 12.8 Hz), 2.02 (quin, 2H, *J* = 6.0 Hz), 1.45 (s, 9H). ^{13}C NMR (100.6 MHz, $CDCl_3$: δ 160.8, 158.5, 156.4, 147.2, 147.1, 124.7, 124.5, 115.9, 114.8, 79.5, 66.1, 38.1, 29.7, 28.6 ppm. HRMS Calcd. for $C_{20}H_{25}N_3O_4$ $[M]^{1+}$: 372.1923, found: 372.1916.

Synthesis of tert-butyl (E)-(3-(4-((4-(3-bromopropoxy) phenyl)diazenyl)phenoxy)propyl)-carbamate, *6*

A solution of **5** (100 mg, 0.27 mmol) and potassium carbonate (186 mg, 1.35 mmol) in dmf (10 mL) was stirred for 5 min at room temperature (RT). Commercially available 1,3-dibromopropane (81 mg, 41 µL, 0.4 mmol) was added and after 90 min of stirring, the reaction mixture was quenched with 20 mL of water. The product was extracted with ethyl acetate (3 × 10 mL) and the organic fraction was washed with brine (2 × 10 mL). The organic portion was dried over $MgSO_4$, filtrated and the solvent removed under vacuum to afford **6** as an orange solid. (127 mg, 95%). ^{1}H NMR (400 MHz, $CDCl_3$): δ 7.91 (d, *J* = 7.6 Hz, 4H) 7.06–6.96 (m, 4H), 4.74 (br, 1H), 4.20 (t, 2H, J = 5.8 Hz), 4.10 (t, 2H, *J* = 6.0 Hz), 3.63 (t, 2H, J = 6.4 Hz), 3.36 (q, 2H, *J* = 5.6 Hz, *J* = 11.57 Hz), 2.36 (quin, 2H, J2 = 6.1 Hz), 2.02 (quin, 2H, *J* = 6.2 Hz), 1.45 (s, 9H) ppm. ^{13}C NMR ($CDCl_3$, 100.6 MHz): 161.0, 160.9, 156.2, 147.2, 147.1, 124.6, 114.9, 114.8, 79.5, 66.2, 65.8, 38.1, 32.4, 30.0, 29.7, 28.6 ppm. HRMS Calcd. for $C_{23}H_{30}BrN_3O_4$ $[M]^{1+}$: 492.1498, found: 492.1485. ^{1}H/^{1}H and ^{1}H/^{13}C correlation were recorded.

Synthesis of tert-butyl (E)-(3-(4-((4′-(3′-(ethylthio)propoxy) phenyl)diazenyl)phenoxy)propyl)-carbamate, *7*

A solution of **6** (724 mg, 1.95 mmol), ethanethiol (173 µL, 2.35 mmol) and potassium carbonate (1.347 g, 9.75 mmol) in dmf (25 mL) was stirred 5 h at RT. Then 30 mL of water were added, the resulting solution was cooled and a yellow precipitate appeared. The solid was filtered, washed with water (3 × 5 mL) and dried under vacuum to obtain **7** as a yellow solid. (635 mg, 69%). ^{1}H NMR (250 MHz, $CDCl_3$): δ 7.86 (d, 4H, *J* = 8.2 Hz), 7.03–6.95 (m, 4H), 4.76 (br, 1H), 4.15 (t, 2H, *J* = 6.2 Hz), 4.10 (t, 2H, *J* = 5.9 Hz), 3.35 (q, 2H, *J* = 6.3 Hz, *J* = 12.3 Hz), 2.74 (t, 2H, *J* = 7.2 Hz), 2.58 (q, 2H, *J* = 7.2 Hz), 2.10 (quin, 2H, J = 7.0 Hz), 2.02 (quin, 2H, *J* = 6.2 Hz), 1.45 (s, 9H), 1.28 (t, 3H, *J* = 5.9 Hz) ppm. ^{13}C NMR (100.6 MHz, $CDCl_3$): 161.3, 161.1, 156.2, 147.0, 146.9, 124.7, 114.9, 79.8, 69.2, 66.8, 38.1, 29.8, 29.3, 28.6, 28.2, 26.2, 14.9 ppm. HRMS Calcd. for $C_{25}H_{36}N_3O_4S$ $[M]^{1+}$: 496.2227, found: 496.2240. ^{1}H/^{1}H and ^{1}H/^{13}C correlation were recorded.

Synthesis of (E)-1-(4-(3-(chloro-l5-azanyl)propoxy) phenyl)-2-(4-(3-(ethylthio)propoxy)phenyl)-diazene, *8*

The deprotection of the amine group was performed following a previously described procedure [39]. 1 mL of concentrated HCl was added dropwise to a flask with **7** (306 mg, 0.65 mmol) in ethyl acetate (5 mL), and the solution was stirred at RT for 1 h. The reaction product was precipitated with hexane. The solid was collected and washed several times with 5 wt % sodium bicarbonate solution and dried under vacuum to obtain **8** as a yellow solid. (203 mg, 84%). ^{1}H NMR (250 MHz, CD_3OD): δ 7.85 (m, 4H), 7.07 (m, 4H,), 4.19 (m, 4H), 3.07 (t, 2H, J = 7.17 Hz), 2.73 (t, 2H, J = 7.03 Hz), 2.56 (q, 2H, J = 7.3 Hz), 2.11 (m, 4H), 1.26 (t, 3H, J = 7.3 Hz). ^{13}C NMR (100.6 MHz, CD_3OD): 162.7, 162.2, 148.4, 148.1, 125.3, 115.8, 67.8, 66.8, 38.9, 30.3, 30.1, 28.7, 26.6, 15.2. HRMS Calcd. for $C_{20}H_{28}N_3O_2S$ $[M]^{1+}$: 374.1902, found: 374.1901.

Synthesis of (E)-4,4′-di(ethanethiolpropanoxy)azobenzene, *12*

Ethanethiol (120 mg, 1.9 mmol) was added to a flask with **11** (402 mg, 0.9 mmol) and potassium carbonate (609 mg, 4.4 mmol) in dmf (20 mL) and stirred at RT overnight. Then, 30 mL of water were added, and the precipitate was collected and washed with water (6 × 5 mL). The isolated solid was dried under vacuum to afford **12** as a yellow solid (205 mg, 56%). ^{1}H NMR (250 MHz, $CDCl_3$): δ 7.87 (d, 4H, *J* = 9.23 Hz), 7.00 (d, 4H, *J* = 9.13 Hz), 4.15 (t, 4H, *J* = 6.35 Hz), 2.74 (t, 4H, *J* = 6.95 Hz), 2.57 (q, 4H, *J* = 7.32 Hz), 4.24 (quin, 4H, *J* = 6.65 Hz), 2.74 (t, 4H, *J* = 6.95 Hz) ppm. HRMS Calcd. for $C_{22}H_{30}N_2O_2S_2$ $[M]^{1+}$: 419.1821 found: 419.1814.

Synthesis of di-µ-chloro-bis(N,N-dimethylbenzylamine-2-C,N) diplatinum(II) complex, $[Pt(dmba)Cl]_2$, 13

The synthesis was carried out adapting a previously described synthesis [40]. To a flask with K_2PtCl_4 (908 mg, 2.19 mmol) in distilled water (20 mL) a solution of *N*,*N*-dimethylbenzylamine in methanol (18 mL) was added, and the resulting mixture was stirred at RT for 2 days. The black/brown solid formed was collected by filtration and was extracted with hot $CHCl_3$ (150 mL). The solvent was evaporated to dryness and the crude was purified by column (SiO_2, $CHCl_3$: AcOEt (9:1)) to obtain **13** as a white solid. (200 mg, 28%). ^{1}H NMR (250 MHz, $CDCl_3$): δ 7.24–7.20 (m, 1H), 7.02–6.81 (m, 3H), 3.89 (s, 2H, J = 27 Hz), 3.01 (s, 6H, J = 23 Hz). ^{195}Pt NMR (128 MHz, $CDCl_3$): -3657.9 ppm.

Synthesis of Pt(dmba)(*8*)Cl, *14*

A previously sonicated suspension of **13** (20 mg, 0.028 mmol) in methanol (10 mL) was added to a solution of **8** (23 mg, 0.056 mmol) and sodium methoxide (25%) (13 µL, 0.056 mmol) in methanol (5 mL) and the resulting mixture was stirred overnight at 50 ºC. Afterwards, the solution was evaporated until the appearance of a solid, which was removed by filtration. The filtrate was evaporated to dryness to obtain **14** as an orange crystalline solid, which was washed with water, ethanol and diethyl ether. (10.8 mg, 25%). ^{195}Pt NMR (128 MHz, $CDCl_3$): − 3706 and − 3303 ppm. HRMS Calcd. for $C_{29}H_{39}N_4O_2PtS$ $[M]^{1+}$: 702.2438 found: 702.2447.

Synthesis of Pt(dmba)(*7*)Cl, *15*

A previous sonicated suspension of **13** (44 mg, 0.060 mmol) in methanol (13 mL) was added to a suspension of **7** (56 mg, 0.118 mmol) in methanol (5 mL) and was stirred overnight at 50 ºC. At that point, the solution was evaporated until precipitation starts. The solid was removed by filtration, and the filtrate was evaporated to dryness to obtain a brown crystalline solid identified as **15**. (31 mg, 30%) ^{1}H NMR (360 MHz, $CDCl_3$): δ 7.91–7.79 (m, 4H), 7.41 (d, 1H, J = 21.6 Hz), 7.09–6.88 (m, 7H), 4.75 (br, 1H), 4.27–4.14 (m, 2H), 4.10 (t, 2H, J = 6.1 Hz), 3.94 (s, 2H, J = 18 Hz), 3.72–3.43 (br m, 2H), 3.41–3.27 (m, 2H), 2.99 (s, 6H, J = 17 Hz), 2.95–2.70 (m, 2H), 2.48–2.21 (m, 2H), 2.07–1.92 (m, 2H), 1.45 (s, 9H), 1.45–1.37 (m, 3H) ppm. ^{13}C NMR (100.6 MHz, $CDCl_3$): 160.9, 160.8, 156.2, 147.6, 147.2, 134.4, 131.8, 125.6, 124.5, 124.1, 121.8, 114.9, 114.8, 79.5, 75.3, 66.3, 66.2, 52.6, 38.1, 33.9, 32.7, 29.7, 28.6, 28.0, 13.4. ^{195}Pt NMR (128 MHz, $CDCl_3$): − 3706 ppm. HRMS Calcd. for $C_{34}H_{47}N_4O_4PtS$ $[M]^{1+}$: 802.2960, found: 802.2952. ^{1}H/^{1}H and ^{1}H/^{13}C correlation were recorded. Anal. Calcd. for $C_{34}H_{47}ClN_4O_4PtS{\cdot}CH_3OH$ (Mr 869.29): C, 48.30; H, 5.91; N, 6.44; S, 3.68. Found: C, 47.38; H, 5.42; N, 6.37, S, 2.81.

Synthesis of Pt_2(dmba)$_2$(12)Cl_2, 16

A solution of **13** (61 mg, 0.08 mmol) in chloroform (17 mL) was added to a solution of **12** (35 mg, 0.08 mmol) in chloroform (10 mL) and the resulting mixture refluxed overnight. Then, the solvent was evaporated to dryness and the obtained oil was dissolved in the minimum quantity of dichloromethane. Subsequently, methanol was added until an orange precipitate appeared which was collected and washed with methanol (2 × 5 mL) and diethyl ether (2 × 5 mL) and dried under vacuum to obtain an orange solid identified as **16** (28 mg, 29%). ^{1}H NMR (250 MHz, $CDCl_3$): δ 7.83 (d, 4H, J = 9.10 Hz), 7.41 (d, 2H, J = 25 Hz), 7.10–6.85 (m, 10H), 4.32–4.09 (m, 4H), 3.94 (s, 4H, J = 20 Hz,), 3.75–3.42 (m, 2H), 3.53–3.16 (m, 2H), 2.99 (s, 12H, J = 17 Hz), 2.52–2.23 (m, 2H), 1.43 (t, 6H, J = 7.71 Hz). ^{13}C NMR (100.6 MHz, $CDCl_3$): 160.8, 147.6, 147.2, 134.4, 131.8, 125.6, 124.5, 124.1, 121.8, 114.9, 66.3, 52.6, 52.5, 33.9, 32.7, 28.0, 13.4. HRMS for $C_{40}H_{54}N_4O_2Pt_2S_2$ $[M]^{2+}$: 536.1494 found: 538.1494. Anal. Calcd. for $C_{40}H_{54}Cl_2N_4O_2Pt_2S_2{\cdot}C_4H_{10}O$ (Mr 1220.31): C, 43.24; H, 5.28; N, 4.58. Found: C, 43.68; H, 5.08; N, 4.64.

Interaction of metal-complexes with biomolecules by mass spectrometry

For the study of the interaction of the metal-complexes with several biomolecules, molecular mass determination were performed by electrospray ionization mass spectrometry at the *SAQ* in the UAB, equipped with a time-of-flight analyzer (ESI-TOF MS) using a Micro Tof-Q Instrument (Brucker Daltonics GmbH, Bremen, Germany) calibrated with ESI-L Low Concentration Tuning Mix (Agilent Technologies), interfaced with a Series 1100 HPLC pump (Agilent Technologies) equipped with an autosampler, both controlled by the Compass Software.

The interaction of metal-complexes with proteins was analyzed in positive mode. For each experiment, 20 µL of sample was injected at 40 µL·min^{-1}; the capillary counter electrode voltage was 4.5 kV; the desolvation temperature was 100 ºC; dry gas at 6 L·min^{-1}. Spectra were collected throughout an m/z range from 800 to 2500. The liquid carrier was an 85:15 mixture of 15 mM ammonium acetate and acetonitrile, pH 7.0.

The proteins used in this work were purchased from Sigma-Aldrich: human serum albumin (A8763), transferrin (T3309), myoglobin (M6036) and cytochrome C (C3484). The complementary oligonucleotides used in this work, OP1 (5′-CACTTCCGCT-3′) and OP2 (5′-AGC GGAAGTG-3′) were purchased from Eurofins MWG Synthesis GmbH (Ebersberg, Germany). The corresponding double-stranded oligonucleotide (DS) was obtained incubating 50 mM solutions of each strand in MiliQ-water at 70 ºC for 2 h and further allowed to cool slowly overnight at room temperature.

Stock solutions of each protein and DS in water were freshly prepared for each experiment. Stock solutions of each complex were prepared in dmso or dmf.

All samples were prepared by incubating the corresponding complex with the biomolecule at the designed ratio (protein:complex 1:1, 1:5 or 1:10) for 24 h at 37 ºC. Then the samples were injected without any further treatment. All samples were injected at least in duplicate to ensure reproducibility.

DNA interaction

CD measurements

Stock solutions of calf thymus DNA (3.5 mM, Sigma Aldrich), TrisHCl (400 mM), and platinum complexes (15 mM) were used to prepare the different samples. The DNA concentration was determined spectrophotometrically at 260 nm by using the molar absorptivity value of 6600 $M^{-1}{\cdot}cm^{-1}$ per nucleotide. The ellipticity values are given in millidegrees (mdeg).

Competitive *DNA-binding experiments with ethidinium bromide*

A solution of calf-thymus DNA (2.5 µM) in TrisHCl (5 mM) was saturated with a solution of Ethidium Bromide (EB) (12.5 µM). Stock solutions of cisplatin and **14** and **15** (5 µM) were used to titrate the DNA solution adding from 0 to a total amount of 100 µM. After each addition, the solution was stirred during 5 min before measurement The fluorescence spectra of each equivalent added to the DNA-EB solution were measured exciting at 520 nm and recording the emission between 550 and 700 nm. The maximum intensity observed was at 608 nm. The spectra were analyzed according to the classical Stern-Voltmer eq:

$$I_0/I = 1 + K_{SV}[Q]$$

where I_0 is the initial intensity of DNA-EB, I is the intensity recorded after adding each equivalent of complex, K_{sv} is the Stern-Voltmer constant and [Q] is the complex concentration. The data obtained were corrected for the dilution effects by means of the OriginPro8 SR7 software (OriginLab Corporation, Northampton, MA, USA).

Cell culture and cytotoxicity assays

Human cancer cells (HeLa) were obtained from American Type Culture Collection (ATCC, Manassas, VA, USA) and were routinely cultured in MEM (modified Eagle's medium) alpha (Invitrogen) containing 10% heat-inactivated fetal bovine serum (FBS) at 37 ºC in a humidified CO_2 atmosphere. The cytotoxicity of each complex was evaluated using PrestoBlue® Cell Reagent (Life Technologies) assay. Stock solutions of each complex were prepared in dmso and dmf. All working concentrations were prepared in MEM alpha medium (at maximum dmso concentration of 0.2%). Cells were seeded in 96 well plates at a density of 5×10^3 cells/well in 100 µl of culture medium and were allowed to grow overnight. After this time, cells were treated with different concentrations (0, 2.5, 5, 10, 25, 50, 100, or 200 µM) of each complex during 24 h and 72 h and then 10 µL of PrestoBlue® was added following the standard protocol. After 3 h incubation, fluorescence (at 590 nm) was measured by a microplate reader (Victor3). The relative cell viability (%) for each sample related to the control well was calculated. The concentration of the compound versus % viability was plotted to produce the dose–response curves, which were analyzed using a logistic sigmoid function fit with GraphPad Prism 6 software. The reported IC_{50} values are the average of three independent experiments with six replicates per concentration level.

Uptake studies of each complex in HeLa cells were carried out in 6 well plates at a density of 2×10^5 cells/well in 1000 µl of culture medium and were allowed to grow overnight. Then, cells were treated with 10 µM of each complex during 3 h. After this time, the cell culture was collected, and the cells were washed twice with PBS. Then, the cells were trypsinized and collected. All the samples were digested with ultra-pure nitric acid overnight and diluted to the suitable dilution to be detected by ICP-MS (Agilent 7500 instrument, at SAQ in the UAB). All the experiments were repeated twice to obtain the percentage of platinum inside de cell from the total.

Results and discussion

Synthesis of azobenzene ligands

The different ligands used contain an azobenzene unit conveniently functionalized to favor metal binding. Ligands **7** and **8** were synthesized following the strategy summarized in Scheme 1.

3-Bromopropylamine Bromhydrate, **1**, was protected in excellent yield as its Boc-carbamate, following a standard procedure [25]. Then, a nucleophilic substitution from a *p*-nitrophenol and the product **2** in basic conditions [38] was carried out, to finally obtain **3** in 54% yield. The product was apparently an oil, which crystallized after 2 days at RT as a white solid. Different strategies were tried in order to achieve the reduction of the nitro group to the corresponding aniline, **4**. Neither Fe in acetic acid and ethanol [41, 42] nor zinc dust attempts worked. In both cases, a mixture of different products together with starting material were obtained. Finally, a hydrogenation succeeded using 10% of Pd/C as the catalyst in the presence of a catalytic amount of acetic acid in H_2 at 2-bar pressure in a Fisher-Porter vessel. Aniline **4** was obtained as brown oil in 85% yield, which was used without further purification in the next step.

An adaption of the synthesis described by J. Kim and co-workers [38] was followed for azobenzene **5** by means of an azo coupling reaction between the corresponding diazonium salt from **4** and an activated phenol. The activation of

Scheme 1. Synthetic strategy for ligands **7** and **8**

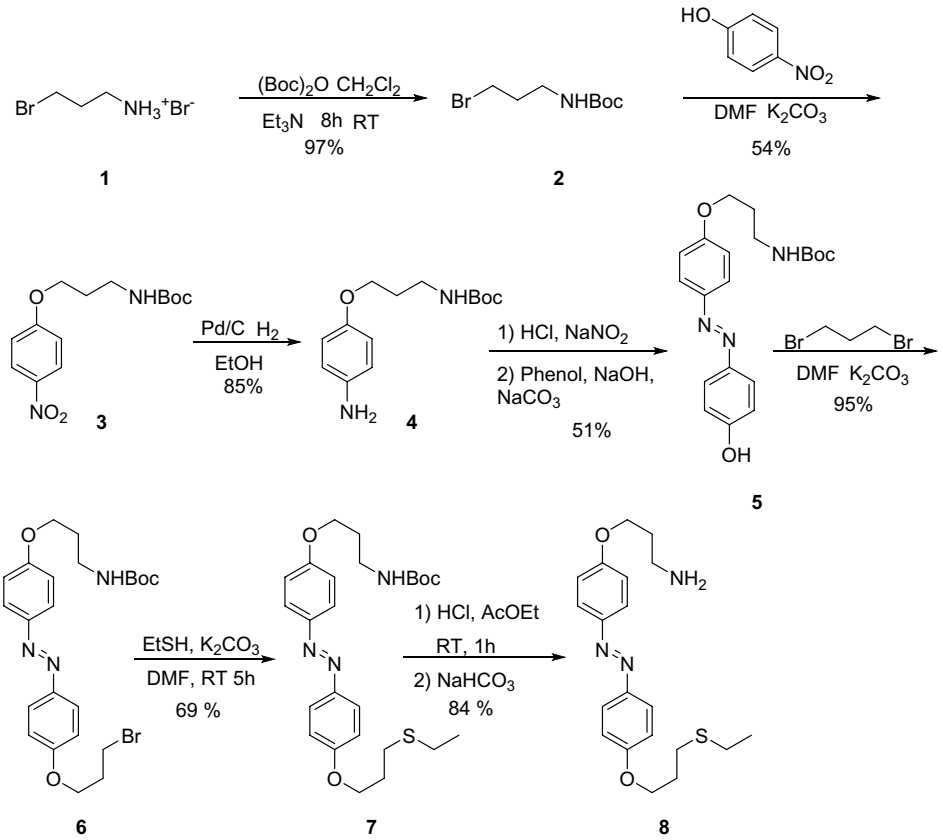

the phenol from its ionized form was required because the neutral molecule is not sufficiently nucleophilic [41, 42]. For that reason, the pH was controlled in order to get mild basic medium to provide the reaction. The reaction took place selectively in the *para* position of the phenol, which attacks the electrophile diazonium salt to generate **5**, as a yellow/light-brown solid, in a 51% yield after recrystallization.

Azobenzene **6** was synthetized in 95% yield by means of a monosubstitution reaction of 1,3-dibromopropane by the corresponding phenolate of **5** using K_2CO_3 as base. Afterwards, the resulting bromide in **6** was substituted by potassium ethanethiolate at room temperature. A yellow solid was obtained in 69% yield which was identified as diazobenzene, **7**. The amine group deprotection in **7** was easily carried out with concentrated HCl at RT, followed by precipitation of the corresponding ammonium salt in hexane. After washing several times with sodium bicarbonate solution, amine **8** was obtained in 84% yield.

Ligand **12** was synthetized starting from 4-aminophenol, **9** (Scheme 2) [35]. Coupling reaction of commercially available **9** in a neat reaction with potassium hydroxide at high temperature yielded **10** as a brown solid in 36%. The

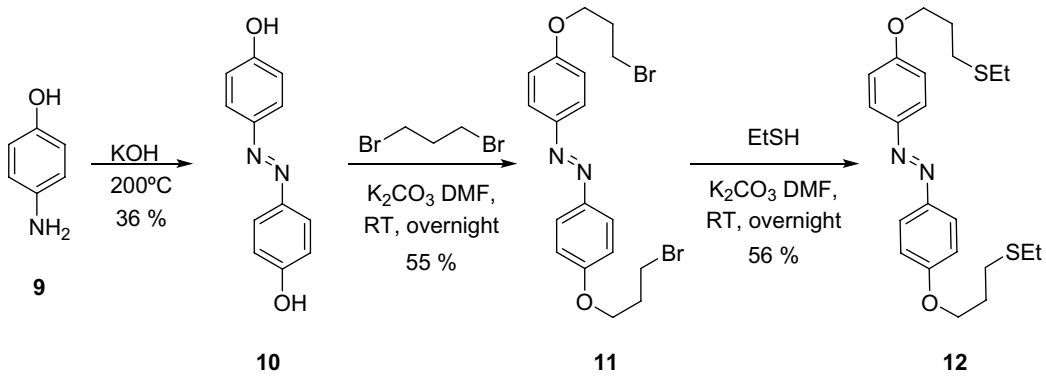

Scheme 2. Synthetic strategy for ligand **12**

synthesis was continued in a similar manner as for **8**, but introducing, in this case, two bromopropyl chains. This double substitution required longer reaction times; up to 19 h instead of 90 min from **5** to **6**. In this way, **11** was obtained as a yellow solid in 55% yield. Finally, the double substitution of both bromide groups by the corresponding thioether in basic conditions gave azobenzene **12** as a yellow solid in 56% yield.

Synthesis of Pt-compounds

The new Pt(II) compounds were synthesized using the previously described ligands. The synthesis and purification of each compound required a specific strategy.

Di-μ-chloro-bis(*N*,*N*-dimethylbenzylamine-2-*C*,*N*) diplatinum(II) complex, $[Pt(dmba)Cl]_2$, **13** (Scheme 3) was prepared as a common platinum(II)-complex precursor. The synthesis was carried out from an adaption of the work by Ryabov and co-workers [40]. After a 2-days reaction of the commercially available starting material K_2PtCl_4 and two equivalents of dmba in a mixture of water/methanol, and column purification a stable dimer **13** was obtained as a white solid. This complex bears *N*,*N*-dimethylbenzylamine (dmba) as bidentate ligand by means of a chelate bond between the nitrogen atom of the amine and a carbon atom of the benzyl group with the platinum(II) center. This chelate ring confers higher stability to the platinum(II)-complex than most other bidentate ligands due to its kinetic inertness [43, 44].

The platinum(II)-complex, **14**, bearing ligand **8** was synthetized as follows. Azobenzene **8** was treated with a previously sonicated solution containing the precursor complex **13** in basic conditions, using sodium methoxide. In this way, complex **14** was obtained in 25% yield, as an orange solid (Scheme 3). The mass spectrum (SI, Figure S21) confirms the formulated complex by means of the observation of a peak that corresponds to $[M\text{-}Cl]^+$. Moreover, this peak is also consistent with the expected isotopic pattern. However, a complex ^{1}H-NMR spectrum was obtained, with several peaks at the aliphatic area. In addition, a super-broad signal was acquired at around − 3000 ppm for ^{195}Pt-NMR experiment (SI, Figure S19). Only an indirect acquirement of the ^{195}Pt-NMR chemical shifts by means of an ^{1}H-^{195}Pt-HMBC experiment revealed two peaks corresponding to different platinum(II)-complexes, − 3706 and -3303 ppm (SI, Figure S20), which are the expected for platinum in the + 2 oxidation state [46].

Two hypotheses regarding possible structures for the synthetized **14** complex were postulated: (a) the complex in solution was completely in a dynamic equilibrium between two or more compounds, which does not allow to obtain a clear ^{1}H-NMR spectrum; (b) two or more isomers were formed in the reaction, which could be also according to the obtained HR-MS data.

In the bibliography, different examples of hemilabile molecules of bidentate ligands are reported, and especially for those ligands with two donor centers with different strengths [45]. In these studies, the hemilabile ligands experience dynamic equilibrium with the Pt(II) center, and the recorded ^{1}H-NMR spectra also show broad signals. In our case, **8** presents two donor centers which could act as hemilabile ligands. In order to prove the first hypothesis (a), different ^{1}H-NMR spectra were recorded at different temperatures. If the complex undergoes a dynamic equilibrium, the change of the temperature will modify its equilibrium constant [45] and, therefore, the ^{1}H-NMR signal distribution. However, no changes were observed in the different spectra recorded neither when the temperature was increased or decreased.

The postulation of the second hypothesis (b) entailed that the reaction of **8** with the platinum(II) precursor, **13**, could evolve into different constitutional isomers. The sulfur atom is softer than the nitrogen atom, as primary amines are hard bases. Consequently, the coordination of the first to the Pt(II) center should be more favorable than the coordination of the latter. However, to verify the existence of different isomers, a new Pt(II)-complex was synthetized. The previously synthetized **7** was used as a ligand, which differs from **8** only in the amine-protection. The protecting Boc group should block the coordination of the nitrogen atom to the metal center, and apparently, only the sulfur atom should coordinate to the Pt(II). The synthesis of this complex was carried out in similar conditions than those used for the synthesis of **14**, but without using sodium methoxide. After an

Scheme 3. Synthesis of [Pt(dmba)(**8**)Cl], **14**

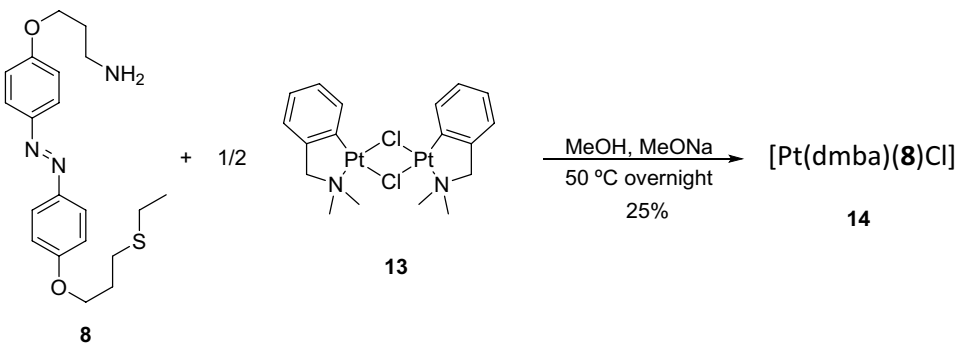

Scheme 4. Synthesis of [Pt(dmba)(**7**)Cl], **15**

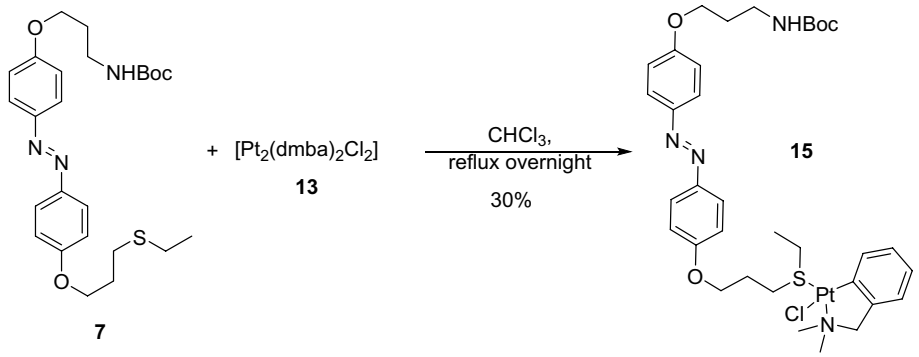

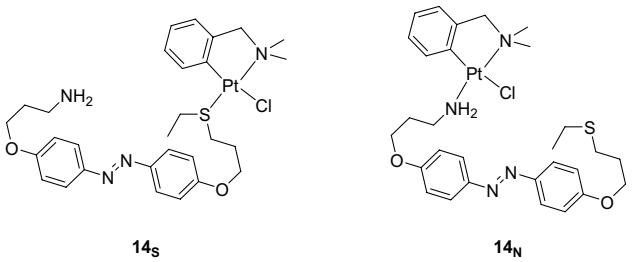

Fig. 1 Proposed structures for both isomers of **14**. According to similar examples in literature, *S*,*N-trans* configuration has been tentatively assigned for Pt complexes in this work [22]. By analogy, $\mathbf{14}_{\mathbf{N}}$ has been also proposed as *N*,*N-trans*

overnight-reaction [Pt(dmba)(**7**)Cl], **15** was obtained in 30% yield as a brown solid (Scheme 4).

The complex was fully characterized by ^{1}H-, ^{13}C{^{1}H}- and ^{195}Pt{^{1}H}-NMR spectroscopy, the corresponding two-dimensional NMR spectroscopy, HR-MS and elemental analysis (SI, Figures S22-S27).

The peak observed in the mass spectrum (SI, Figure S27) was consistent with the complex formulated, exhibiting the expected isotopic pattern. The ^{1}H-NMR spectrum suggested the coordination of the platinum atom to the sulfur, because the aliphatic signals near to the coordinated atom are shifted and broader. Consequently, their multiplicity cannot be observed, and neither the ^{195}Pt-^{1}H couplings as satellites (SI, Figure S22). The ^{195}Pt-NMR chemical shift was – 3706 ppm, which fits with one of those two found for **14**. Therefore, one isomer of **14** corresponds to a complex bound to the sulfur atom of the thioether group, $\mathbf{14}_{\mathbf{S}}$. Consequently, the other isomer might be that one coordinated to the amino group, $\mathbf{14}_{\mathbf{N}}$ (Fig. 1).

A dinuclear complex, **16**, bearing azobenzene **12** was synthetized. This reaction was performed with an equimolar amount of the precursor complex **13** in chloroform. After precipitation with methanol, dinuclear complex **16** was isolated by simple filtration as an orange solid in 29% yield (Scheme 5).

The formation of complex **16** was corroborated by different techniques. By comparison of ^{1}H-NMR spectra of free ligand **12** and complex **16**, the signals corresponding to the neighboring thioether protons, H-3 and H-4, are shifted to the lower field. This effect can be also observed for protons in beta position though in a minor degree (SI, Figure S33). ^{195}Pt NMR chemical shift at -3705 ppm was obtained indirectly by ^{1}H-^{195}Pt-HMBC recorded spectrum (SI, Figure S34). This chemical shift corroborates the coordination

Scheme 5. Synthesis of dinuclear complex **16** from azobenzene **12** and precursor **13**

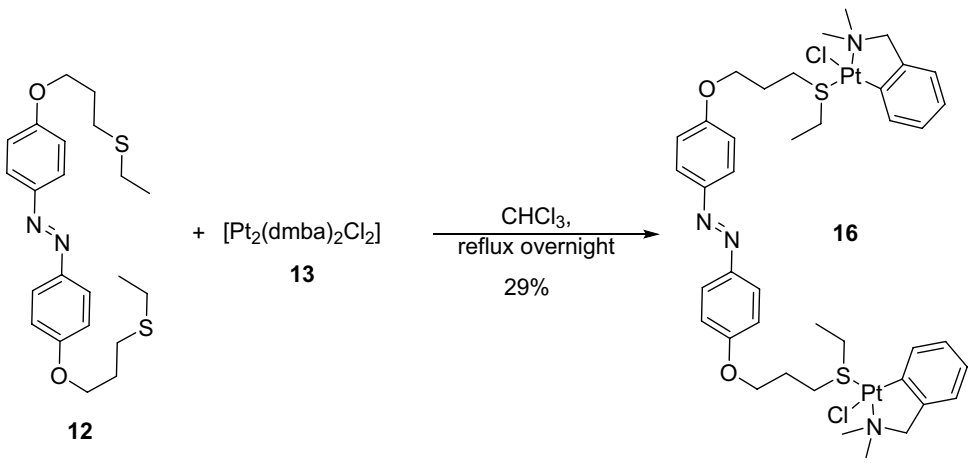

sphere of the complex. In addition, the mass spectrum showed a peak that corresponds to $[M\text{-}Cl\text{-}Cl]^{2+}$. Moreover, its expected isotopic pattern was observed (SI, Figure S32). All of these results allow us to confirm the formulated-complex, as long as its purity by elemental analysis.

Photochemistry

Azobenzene-derivative molecules, as explained before, are well-known to have a characteristic reversible photoisomerization from its *trans*-to-*cis* isomeric form and vice versa. For that reason, the photophysical properties of the **7**, **8** and **12** synthetized azobenzene ligands and their corresponding Pt(II)-complexes (**14**, **15** and **16**) were investigated. The type of ligands used in this work contain, in both rings of the azobenzene moiety, an ether group substituted in *para* position, and therefore both rings show equal electronic properties. However, the substituted group in each chain could influence their kinetic photoisomerization by means of, for example, steric impairments.

The absorption spectra of the thermally stable *trans*-isomer of ligands **7**, **8** and complexes **14** and **15** were recorded (Fig. 2). As expected, all these compounds show the same absorption bands, which are characteristic of azobenzene-type compounds: a very intense $\pi \rightarrow \pi^*$ transition band localized at 358 nm, together with a much weaker $n \rightarrow \pi^*$ band around 450 nm, in the blue-green region of the visible spectrum. The spectra obtained for **14** and **15** suggest that the azobenzene moiety is far away from the metallic center, as they are very similar to those recorded for the free ligands. Despite both bands are found in the ligands and in the complexes, this demonstrates that these units are not electronically coupled in the ground state of complexes **14** and **15**.

Azobenzene derivatives can undergo *trans*-to-*cis* isomerization upon irradiation at the wavelength where the $\pi \rightarrow \pi^*$ absorption band of the *trans*-isomer appears [21]. Upon irradiation for 1 min at 365 nm, diluted solutions of the *trans*-isomers of **7**, **8**, **14** and **15**, were analyzed by UV–vis in ACN as solvent. In all the cases the photostationary states (PSS), *i.e.,* the maximum amount of the *cis*-isomer that can be achieved, were obtained (Fig. 3). The *cis*-isomer spectra for all compounds show the same noticeable differences with the corresponding *trans*-isomer spectra: (a) intensity decrease and hypsochromical shift of the $\pi \rightarrow \pi^*$ electronic transition band, which are ascribed to the loss of planarity of the *cis*-azobenzene moiety; and b) a slight increase of the $n \rightarrow \pi^*$ transition absorption band, at 450 nm.

Both complexes, **14** and **15**, present a characteristic band around 280 nm, which seems to be related to the dmba ligands of the complexes (Fig. 3a, b). Although this band is not shifted in their *cis*-isomeric form regarding to that of their *trans*-isomer, the intensity is slightly higher. Moreover, the absorption bands that correspond to the azobenzene moieties of the *cis*-isomers of **14** and **15** are overlapped with those of their respective ligands, **8** and **7**. Therefore, these results corroborate that the metal-complex and the azobenzene moiety are not electronically coupled in the *cis*-state.

As expected for azobenzene-derivative switches, *cis*-to-*trans* back isomerization of ligands *cis*-**7** and *cis*-**8**, were observed as well as for complexes *cis*-**15** and *cis*-**14** both

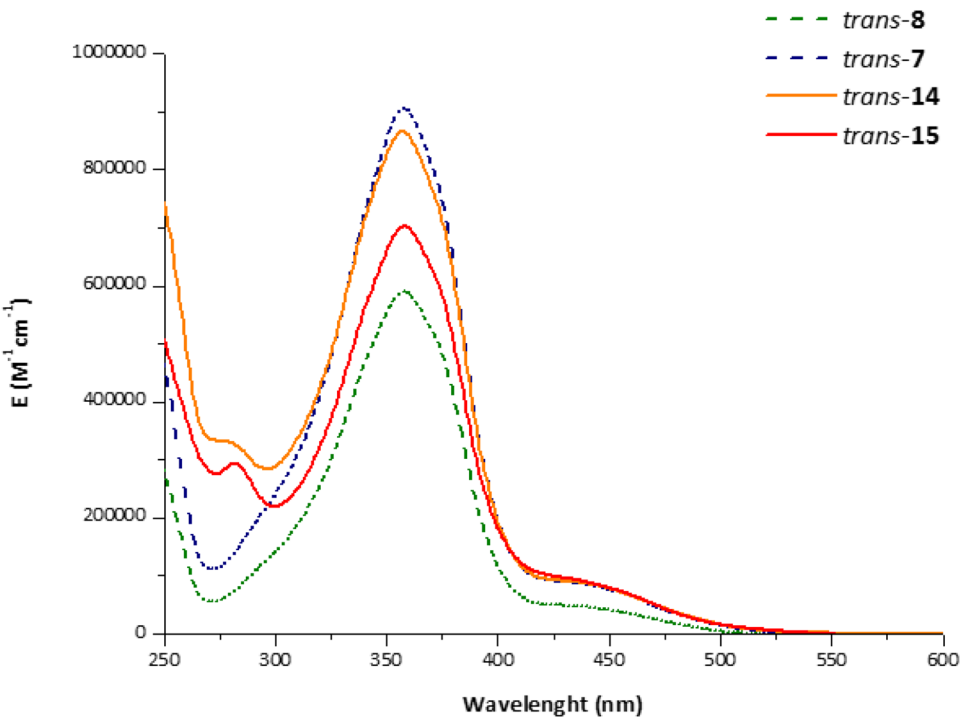

Fig. 2 Absorption spectra of compounds **7**, **8**, **14** and **15** in ACN. Measurements were carried out at low concentrations ($\sim 10^{-5}$ M) to minimize aggregation processes

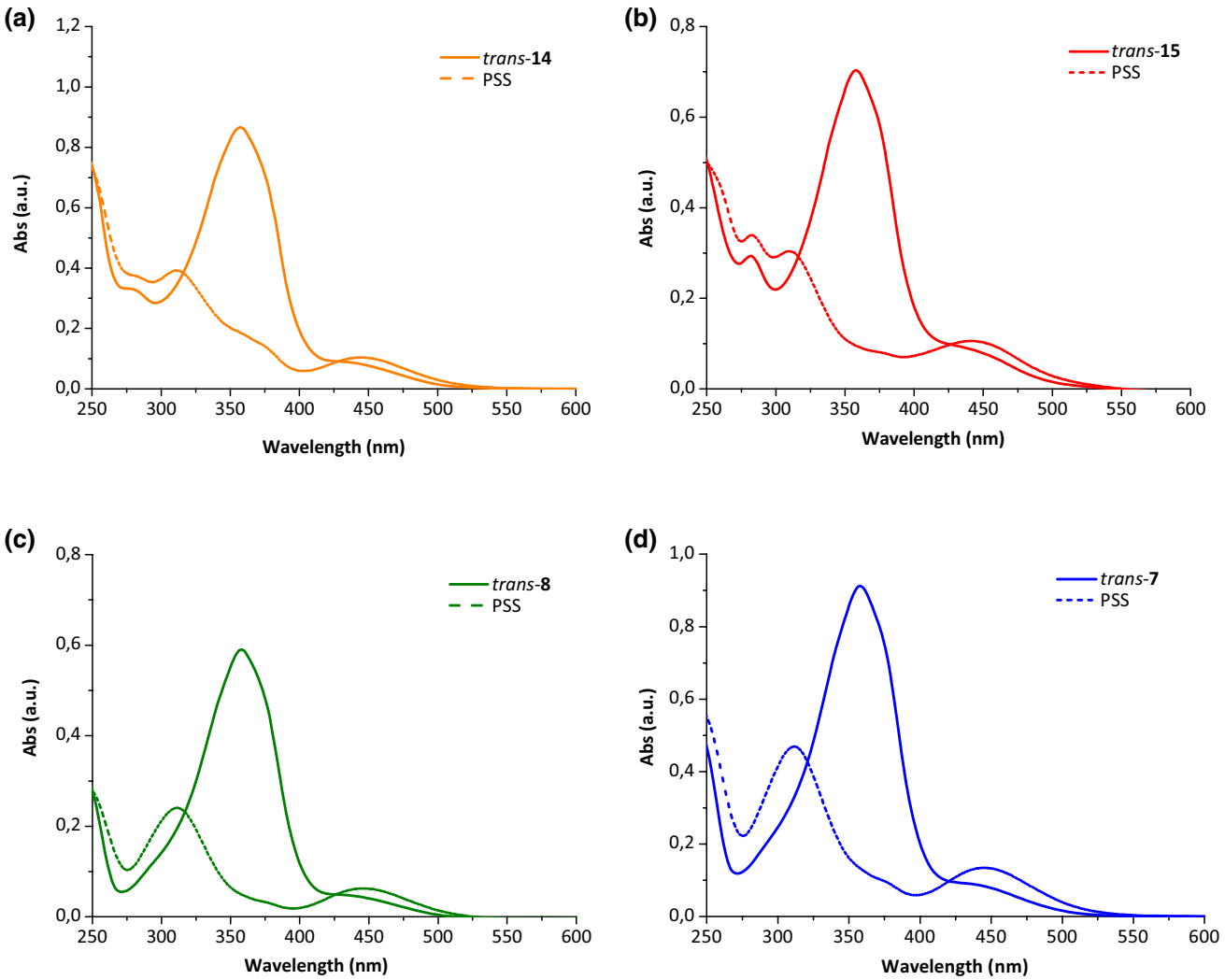

Fig. 3 Absorption spectra in ACN of the *trans*-isomer and the PSS for complexes: (**a**) **14**, (**b**) **15**, and their corresponding ligands: (**c**) **8** and (**d**) **7**

by photoexposition and thermally. In all cases, quantitative conversion to their *trans*-isomers was observed.

Due to the putative different reactivity of both Pt(II)-isomers, and to check the stability of the *cis* isomer, the thermally *cis*-to-*trans* isomerization process was studied. For that, back isomerization from the PSS to the more stable *trans*-isomer was followed by UV–vis absorption spectroscopy. After irradiation, the spectra were recorded periodically and furtherly, the values of the absorbance at the $\pi \rightarrow \pi^*$ band, *i.e.* at the maximum absorption of the *trans*-isomer, were plotted over time (SI, Figures S36 and S37). The data was adjusted to a monoexponential function, indicating that this process follows a first-order kinetic rate. The equation derived from this adjustment allowed to obtain the rate constant of each isomerization and also the half-lives of each *cis*-isomer (Table 1).

Table 1 Parameters of the thermal *cis* → *trans* back isomerization in ACN of compounds **7**, **8**, **14** and **15**

Compound	$k_{cis \rightarrow trans}$ (s^{-1})	$t_{1/2}^{cis}$(h)
7	6.0×10^{-5}	3.2
8	$3{,}8 \times 10^{-6}$	50,0
14[a]	$2{,}0 \times 10^{-5}$	9,6
15	1.5×10^{-5}	12.8

a) Values for 14 were listed just to give a notion of their order of magnitude as they have been calculated from a mixture of two species 14_S and $14_{N.}$

All the half-live of the *cis*-isomers calculated are in the timescale of hours at room temperature. However, some differences can be observed among them. The half-live of *cis*-**7** is shorter than that of **8**. This might be attributed to the polarity of the molecule. On one hand, azobenzene-**7** contains a Boc and a thioethane groups in the alkyl chains, while **8** exhibits different polarity, due to the amine group (Scheme1). Because the back-isomerization rate depends on the polarity of the solvent [50], the influence of the substituent groups in azobenzene molecules seems to be essential.

Differences between the rate constants of the free azobenzene **7** or its corresponding complex **15** might be ascribed to the bulkier complex introduced in one of the phenyl groups of the azobenzene, which seems to provoke a decrease of the *cis*-to-*trans* thermal back isomerization rate [24].

Aiming to quantify the amount of *trans*- and *cis*-azobenzenes in the PSS, ^{1}H-NMR was considered a good choice because azobenzenes present different electronic configuration and polarity at each isomeric form, thus possessing unique or specific NMR spectra. With the intention of obtaining comparative results with the study by UV–vis absorption spectroscopy, it was decided to use CD_3CN as

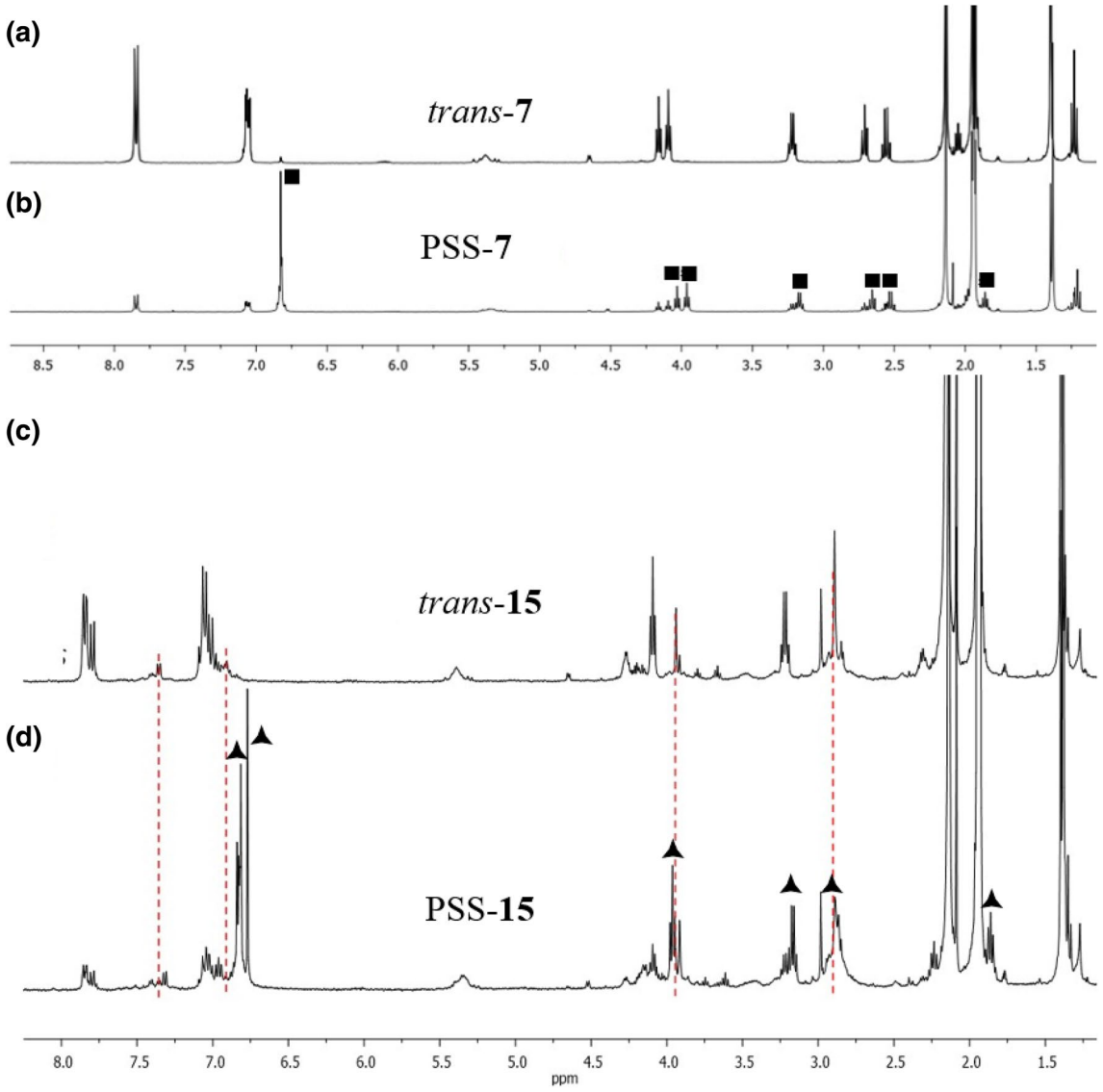

Fig. 4 **a** ^{1}H-NMR spectrum of ligand *trans*-**7** in CD_3CN, 298 K. b) ^{1}H-NMR spectrum after irradiation of *trans*-**7** at 365 nm (PSS-**7**), signals corresponding to *cis*-**7** and *trans*-**7** isomers are visible. c) ^{1}H-NMR spectrum of ligand *trans*-**15** in CD_3CN, 298 K. d) ^{1}H-NMR spectrum in CD_3CN, 298 K of complex **15** after irradiation at 365 nm (PSS-**15**). (■= Signals assigned to the *cis*-**7** isomer. = ʌsignals assigned to *cis*-**15**)

solvent. Though both, ligand **7** and complex **15**, were totally soluble in CD_3CN, **8** and **14** showed low solubility in this solvent, therefore we decided to focus our study on **7** and **15** (Fig. 4).

The ^{1}H-NMR spectrum of PSS-**15** in CD_3CN (Fig. 4d) shows some broad signals that correspond to those protons that are close to the metal-center, due to their long relaxation time. Accordingly, the signals corresponding to the protons distant to the metal center can be observed clearly. In addition, in the aromatic region, a unique signal about 6.8 ppm related to the aromatic protons of the *cis*-**7** (Fig. 4b) was obtained, while two different signals for these protons were obtained for *cis*-**15** (Fig. 4d), showing some loss of symmetry that indicates the preferred coordination of the metal center to one of the two chains of the ligand. Moreover, aromatic protons of the azobenzene moiety of the *cis*-**15** were assigned by a 2D-NOESY experiment. Both signals at 6.85 and 6.80 ppm are correlated by distance with those at 3.99 and 4.18 ppm, related to the α-oxygen protons (SI, Figure S35).

Once the specific signals were identified, the *cis*:*trans* ratios in the PSS were determined as 3:1 for complex **15** while 4:1 for ligand **7** (SI, Figures S38 and S39, respectively). This similarity reveals that their direct *trans*-to-*cis* photoisomerization is not noticeably affected by the introduction of the Pt(II) center.

Due to their poor solubility in ACN, the photochemical characterization of **12** and the dinuclear complex **16** was carried out in CH_2Cl_2. Absorption spectra of both compounds overlap, indicating that the ligand-to-metal coordination does not modify the absorption of the azobenzene moiety (Fig. 5). Both compounds show a very intense $\pi \rightarrow \pi^*$ transition band localized at 358 nm and a much weaker $n \rightarrow \pi^*$ band around 450 nm being characteristic of azobenzene-type bands.

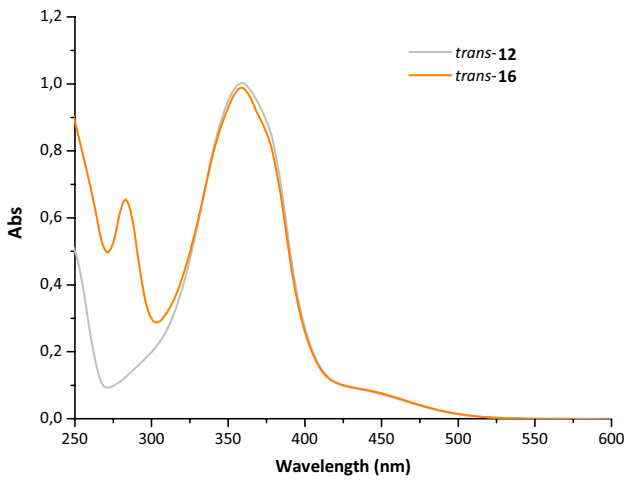

Fig. 5 Normalized absorption spectra of compounds **12** and **16** in CH_2Cl_2. Measurements were carried out at low concentrations to minimize aggregation processes (~ 10^{-5} M)

Next, the *trans* to *cis* photoisomerization was carried out, at 365 nm, for ligand **12** and the corresponding dinuclear complex **16**. Only 1 min of irradiation was required to achieve the PSS for both **12** and **16** (SI, Figure S40). Although this experiment was performed in a different solvent, CH_2Cl_2 instead of ACN, no effect of the solvent was observed in the *trans* to *cis* photoisomerization. However, the kinetic values of the photo-back isomerization show that the half-life values for *cis*-**12** and cis-**16** are shorter than the values reported above for ligand **7** and its corresponding Pt(II)-complex **15** (Table 1). However, these values are related to the photo-exposure of the solution to light, being this a faster reaction than the thermal-back isomerization. Also, the differences in values could be related to the solvent, with different polarity and viscosity than ACN [25].

Nevertheless, these values show again a proportionality between the kinetic constants of *cis*-**12** and *cis*-**16**. The *cis* to *trans* back-isomerization for the *cis*-azobenzene coordinated to Pt(II) center, **16**, proceeds slower than for the free azobenzene, **12**. Therefore, again the Pt(II) center might modify the kinetics of the isomerization process.

Biological assessments

The in vitro antitumoral activity of complexes **14** and **15** were investigated in human cells from the epithelial cervix, HeLa cell lines, which present adenocarcinoma disease. These complexes are soluble enough in a < 0.1% dmso dilution in H_2O required for these experiments. The in vitro anticancer activity was evaluated by means of two experiments: the determination of their cytotoxicity, by calculation of the IC_{50} value; and measurement of the uptake in HeLa cells of each complex.

Cytotoxicity

The IC_{50} value is an indicative of the cytotoxicity of a complex. Additionally, these values can be compared among themselves and with that of cisplatin (or another reference compound), which is used as a model in cytotoxicity studies.

Table 2 summarizes the IC_{50} values calculated for each platinum(II)-complex and ligand reported in this work with the aim of evaluating the effect of the azobenzene ligands. In addition, and because dmso is known to significantly modify the activity of some metal-based anticancer agents [54], the IC_{50} values of complexes **14** and **15** were determined in dmso and in dmf media. Besides, to cover the possibility of dmso displacement of azobenzene ligands, a homologous complex [Pt(dmba)(dmso)Cl], **17** [54], was also tested (Table 2).

Table 2 IC_{50} values measured for ligands and complexes of this work and cisplatin towards HeLa cells at 24 h and 72 h

Entry	Compound	solvent	IC_{50} (24 h)	IC_{50} (72 h)
1	**7**	dmso	> 200	> 200
2	**8**	dmso	24 ± 1	18 ± 2
3	**14**[a]	dmso	11 ± 2	4.9 ± 0.6
4	**15**	dmso	41 ± 6	37 ± 4
5	**15**	dmf	5 ± 2	4.0 ± 0.1
6	**17**[a]	dmso	18 ± 4	13 ± 2
7	cisplatin	water	20	4

[a]IC_{50} values for **14** and **17** in dmf are very similar with those obtained in dmso

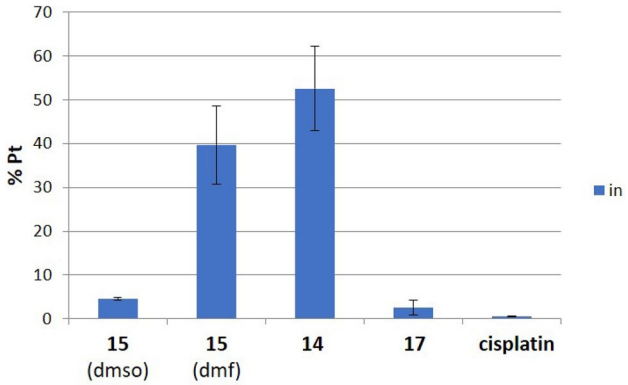

Fig. 6 Percentage of Pt(II) inside HeLa cells after uptake studies with 10 μM of complex exposure for 3 h. Samples were analyzed by ICP-MS after being digested with ultra-pure concentrated nitric acid. The stock solution was also measured and set as 100% of the amount of platinum used, together with the amount "external-platinum". Complexes **14** and **17** are containing dmso as a solvent

First, cytotoxicity for ligands **7** and **8** was checked. As shown in Table 2, while **7** does not exhibit high cytotoxic activity, **8** shows IC_{50} values in the micromolar range. Interestingly, the Pt(II)-complex, **14**, bearing ligand, **8**, presents better values of IC_{50}. Therefore, it can be concluded that the complexation of the azobenzene ligand enhances its cytotoxic activity.

Although no influence of solvent was detected for **14** (Figure S41), **15** showed notable differences depending on the solvent (Table 2, entries 4 and 5). Complex **15** presents much better results in dmf than in dmso. This fact could be attributed to the putative dmso influence removing the azobenzene or maybe the chloride ligand, resulting in a less active complex.

IC_{50} values were calculated at two different exposure times: 24 h and 72 h. However, these values do not differ so much among them, indicating that the activity of all the studied compounds occurs in the first 24 h. Only in the case of **14** a slight improvement of the IC_{50} value was observed after 72 h of complex exposition (Table 2, entry 3). Interestingly, **14** in dmso and **15** in dmf (Table 2, entries 3 and 5) show better IC_{50} values than cisplatin for those experiments at 24 h of complex exposition. However, the values are similar after 72 h, suggesting that the activity of cisplatin is kinetically slower than that of our synthetized-complexes, **14** and **15**.

The molecular switch character of azobenzenes is well known and the opportunity it represents in the field of bioscience [55]. Therefore, it seemed reasonable to assess whether the activity of the Pt-complexes depended on irradiation. To this aim, **14** was taken as a model and it was submitted to three different circumstances: (a) a cell-plate was treated with **14** for 72 h avoiding any exposure to irradiation; (b) a second cell-plate was treated with the corresponding dose of **14**, was irradiated at 365 nm for 5 min and afterwards was incubated in the dark for 72 h; (c) the third cell-plate was irradiated at 365 only after 72 h of incubation. Disappointingly, although slightly differences on the cell viability for 1 μM dose of **14** can be observed, they were not relevant enough (Figure S42).

Uptake assessment

For the uptake studies, cells were treated with each complex at 10 μM for 3 h. Then, the amount of platinum in the cell culture and the cell pellets were quantified by ICP-MS.

The amount of platinum measured inside the cells was different for each complex (Fig. 6): while **14** in dmso and **15** in dmf show the major quantity inside the cell, the amount of the other complexes (**17**, cisplatin and **15** in dmso) is very low.

As previously observed, the activity of complex **15** showed a certain dependence on the medium used, dmso or dmf. Here, the uptake of the complex in the cells was practically avoided when dmso was used as a solvent. Taking together these observations, it seems reasonable to postulate that the low uptake of the complex could be one of the reasons of the decrease of the cytotoxic activity in dmso, compared with that obtained when dmf was used as a solvent (Table 2). However, the use of dmso as a solvent for the uptake studies with **14** did not have the same effect as for **15**. The percentage of Pt(II) inside the cells when they were treated with **14** in dmso was about 53% of the total dose (Fig. 6). This fact suggests that the presence of the free amine in **14** may play a decisive role during the internalization of the complex. Moreover, this conclusion could also explain the activity of ligand **8**. Low quantities of Pt(II) were detected inside the cells when they were treated with

complex **17**. This result suggests that azobenzene ligands, **7** and **8**, might be critical in the internalization process.

DNA-binding studies

The anticancer activity of Pt(II)-complexes is attributed to DNA-binding, being this one of the proposed mechanisms of action of cisplatin [56]. For that reason, the DNA interactions of **14**, **15** and **17** were studied. These studies were carried out by circular dichroism (CD) and fluorescence measurements using calf-thymus DNA.

Circular dichroism measurements Calf-thymus DNA (ct-DNA) presents a characteristic feature of the CD spectrum with small amplitude bands: a positive band *ca.* 280 nm and a negative one *ca.* 245 nm [29]. Modifications in the CD spectrum are attributed to DNA conformational changes because of drug interactions with the biomolecule [57]. Only minor changes in the CD spectrum are attributed to monofunctional platinum(II) adducts, while more dramatic changes are related to bifunctional adducts [60].

The interactions of both complexes, **14** and **15**, with DNA were studied for the *trans*- and *cis*-isomers. *Cis*-configurations were obtained after irradiation of the stock solutions of each complex before being added to the corresponding DNA solution. Moreover, to ensure that the *cis*-isomer was present, the solutions with DNA and the corresponding complex were also irradiated during the experiment. A blank sample of DNA was also irradiated to guarantee its stability under UV light. The corresponding experiment with **15** was achieved in acetonitrile/water solvent, while those with **14** and **17** were carried out in dmf/water.

Different reactivity was measured for *trans*- and *cis*-**14** (Fig. 7, a and b). While modifications of the initial spectrum of the DNA by the *trans*-isomer complex were independent in the [14]/[DNA] ratio, the experiment performed with *cis*- **14** showed a decrease in the positive band dependent on the [14]/[DNA] ratio. The results show minor changes in the CD spectra when *trans*-**15** was incubated with calf thymus DNA. Slight changes were observed for the *cis*-**15** at high [15]/[DNA] ratios (Fig. 7c, d). However, when **17** was incubated with DNA, no changes in the CD spectrum of the ct-DNA were observed, suggesting that **17** does not induce conformational changes in the helicity of DNA (Fig. 7e).

Interestingly, the comparison of the behavior of **17** with some of the changes observed for both **15** and **14**, can indicate that azobenzene ligands should be involved in the interaction with DNA, because when the ligands are replaced by a dmso molecule, *i.e.* for **17**, no changes in the CD spectra are observed.

Competitive DNA-binding experiments with ethidinium bromide Although azobenzene ligands are not known as classical DNA intercalating agents, one promising feature of some platinum(II)-complexes is their intercalation with DNA [61]. For that reason, the potential intercalation abilities of **14**, **15** and **17** were studied by fluorescence experiments by means of a conventional competition experiment with Ethidium Bromide (EB). As expected for cisplatin, complex **17** did not show any changes in the fluorescence spectra (SI, Figure S43 c and d). This result indicates that **17**, despite not intercalating with DNA, it could interact through other mechanisms. Thus, a more extensive study would be required. Although **14** and **15** exhibit a certain degree of intercalation into DNA, their calculated Stern–Volmer quenching constants (K_{SV}) are $1.76{\cdot}10^3$ M^{-1} and $3.46{\cdot}10^3$ M^{-1}, respectively. These values indicate that these complexes are very weak intercalators [61]. The apparent binding constant for these complexes was not calculated because 50% of the initial fluorescence was not reached [62].

Interaction of the complexes with proteins

To evaluate the interaction of the synthesized complexes towards the main proteins in blood stream and other ones related to metal detoxification, complexes **14** and **17** were solubilized in dmso and incubated at 37 ºC with myoglobin, cytochrome C, transferrin and albumin (HSA) at different protein:Pt ratios and followed by ESI–MS (Fig. 8 and Tables S2 and S3). Interestingly, not all the proteins showed the same reactivity with the studied platinum(II) complexes. Notice that since dmso was used as solubilizing solvent, some peaks related to the interaction of **14** and **17** with some of the studied protein showed a dmso molecule coordinated to the metal moiety.

The results obtained show poor interaction of **14** with proteins. No peaks related to covalent binding of the complex to the protein were observed for the incubations with cytochrome C and HSA (Fig. 8b, c). Moreover, the peak of the intact myoglobin was the major one recorded in the mass spectrum when incubating **14** with the protein. At low protein:Pt ratios, a variety of species with one Pt(II)-adduct and different types of ligands attached were observed. However, the main species observed are those peaks related to the protein with one molecule of **14** attached without the azobenzene and the chloride ligands, but with a coordinated dmso, and with that without azobenzene ligand and with a coordinated dmso (Fig. 8a). This variety of species can be explained when considering that **14** is formed by two isomers, $\mathbf{14_S}$ and $\mathbf{14_N}$, thus the first one should have more affinity for Cys residues, while the second for His. Additionally, **14** interacts with transferrin forming Pt(II)-adducts with up to 3 platinum moieties attached to the protein. These adducts correspond to the Pt(II) and the dmba ligand, once released the azobenzene and chloride ligands. However, the

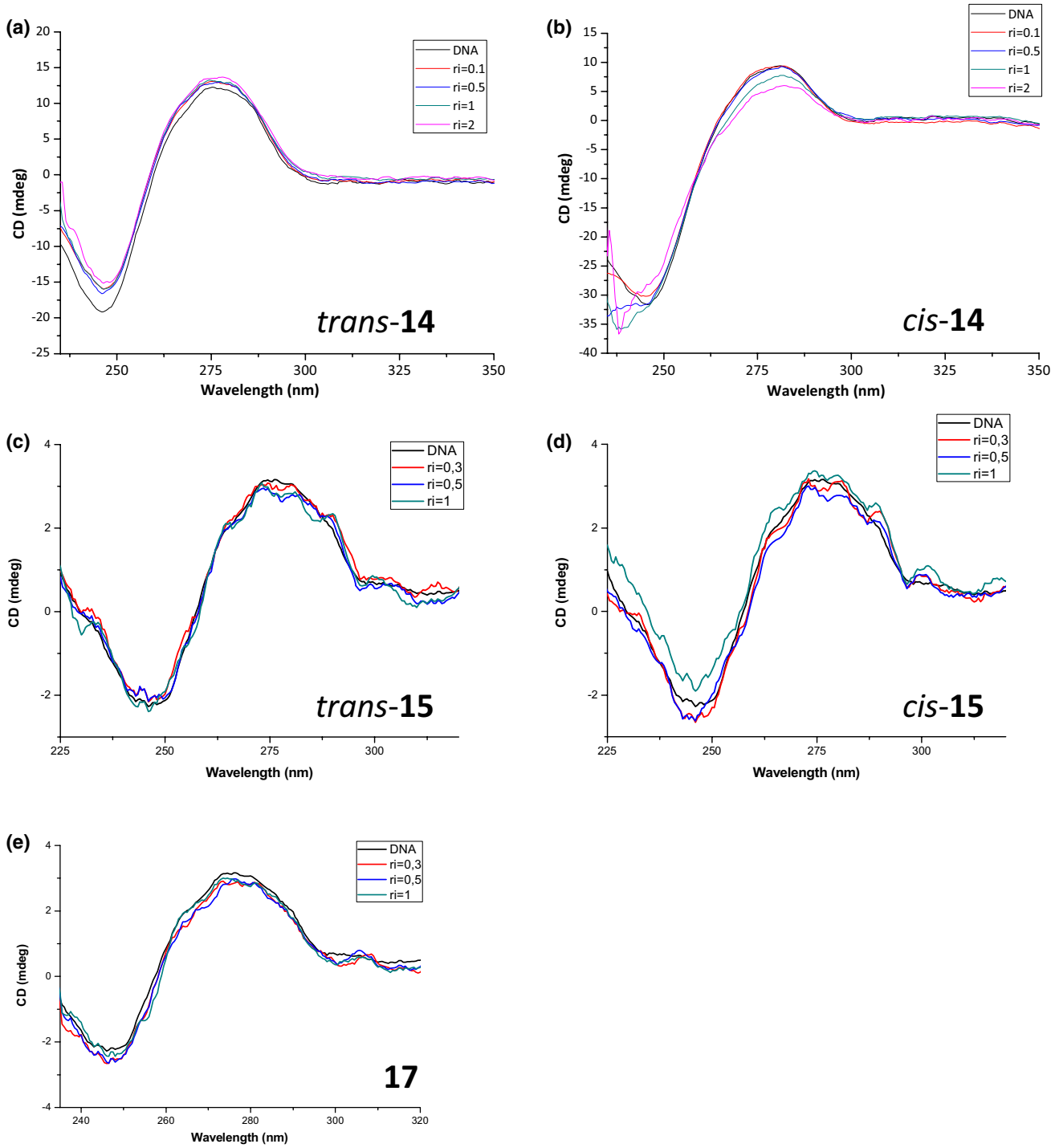

Fig. 7 Circular dichroism spectra of calf thymus DNA incubated with: (**a**) *trans*-**14** and (**b**) *cis*-**14**. In both cases, the concentration of ct-DNA was 50 μM in 10 mM Tris–HCl and 50 mM NaCl, while the complex was ranging from 0 to 100 μM. **c** *trans*-**15** and (**d**) *cis*-**15**. In both experiments, the concentration of ct-DNA was 30 μM in 10 mM Tris–HCl and 50 mM NaCl, while the complex was ranging from 0 to 30 μM. All experiments were carried out at T = 296 K and pH = 7.4

main peak observed in the mass spectra corresponds to a one Pt(II)-adduct (Fig. 8c and SI, Table S1).

The interaction of **17** with the selected proteins was also studied, at different protein:Pt molar ratios (1:1, 1:5 and 1:10) (Table S2). This complex, in contrast with **14**, interacts with all the studied proteins. Only minor peaks were detected with platinum(II)-adducts with cytochrome C in the mass spectra recorded, being the intact protein the

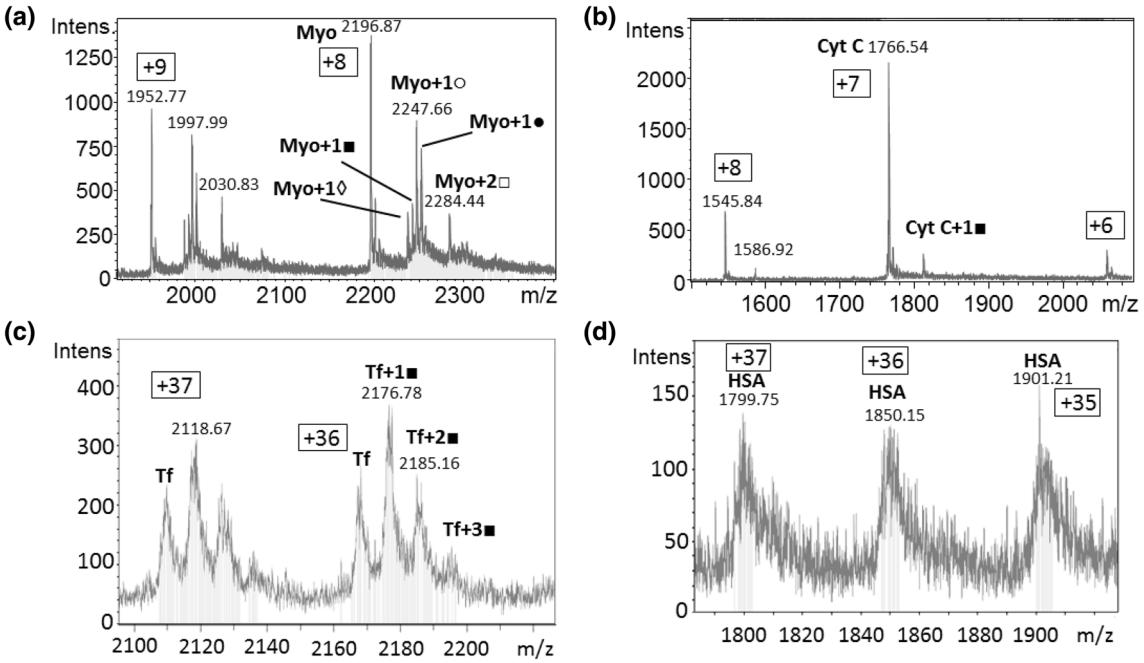

Fig. 8 Mass spectra of **14** recorded after incubation for 24 h at 37 °C with (**a**) myoglobin (Myo) and (**b**) cytochrome C (Cyt C) at a 1:10 (protein:Pt) molar ratios, (**c**) transferrin (Tf) at a 1:5 (protein:Pt) molar ratios and (**d**) human serum albumin (HSA) at a 1:1 (protein:Pt) molar ratios. The numbers proceeded by the "+" symbol in the boxes denote the charge state of the peaks. The notation "+*n*○", where n is a number after the name of the protein, denotes a mass increase corresponding to the addition of "n" molecules of complex **14** to the protein after the elimination of chloride and azobenzene (**8**) ligands, and the coordination of one dmso (738.25–409.01 + 78.1 mass units at the corresponding charge state); the notation "+*n*■" indicates a mass increase corresponding to the addition of "n" molecules of complex **14** after elimination of chloride and azobenzene (**8**) ligands (738.25–409.01 mass units at the corresponding charge state); the notation "+*n*◊" indicates a mass increase corresponding to the addition of "*n*" molecules of complex **14** after elimination of azobenzene (**8**)) ligand (738.25–373.51 mass units at the corresponding charge state); the notation "+*n*●" indicates a mass increase corresponding to the addition of "n" molecules of complex **14** after elimination of azobenzene (**8**)) ligand, and the coordination of one dmso (738.25–373.51 + 78.1 mass units at the corresponding charge state); the notation "+*n*□" indicates a mass increase corresponding to the addition of "n" molecules of complex **14** after elimination of chloride ligand (738.25–35.5 mass units at the corresponding charge state)

major peak even at a 1:10 protein:Pt molar ratio. When **17** interacts with myoglobin (that contains only His, without Cys residues), major species with the complex after the release of chloride ligands were detected. This behavior can be attributed to the presence of only His residues in this protein, facilitating the release of the weakest ligand in the complex, while the S-donor ligand of the initial complex has not been practically replaced. Regarding the interaction of complex **17** with transferrin and HSA, only the mass spectra of the samples incubated at 1:1 protein:Pt molar ratio were obtained. Higher concentrations of complex in solution may cause the destruction of the protein. In both cases, the main peaks detected when both proteins interact with **17** showed the total release of chlorine and dmso ligands, as expected due to the presence of His in Cys residues in both proteins.

When comparing the behavior of both complexes against proteins, it can be observed a higher integrity of **14** than of **17** in the presence of proteins. Interestingly, when **14** interacts with the proteins studied, the release of chloride and of the azo-ligand **8** is required, while only dmso is maintained bound to the platinum moiety. This means that the stability of the complex in front of proteins is high enough and that the only way for them to interact requires the practically total destruction of the complex.

On the contrary, the interaction of **17** with the proteins exhibits certain selectivity. The interaction of proteins containing His required the release of chloride, while with those containing also Cys, the release of dmso was also observed. This particular behavior was also observed in other Pt(II) complexes containing similar ligands, suggesting certain lability of the ligands [63].

Conclusions

The synthesis and characterization of three new azobenzene ligands and of their corresponding platinum(II) complexes revealed that Pt(II) complexation can improve the half-life of their less thermodynamically favored *cis* isomers in respect to that of the free ligands. The *cis–trans* azobenzene ratio

in the photostationary state (PSS) of ligand **7** and its corresponding platinum(II) complex, **15**, revealed the differentiated influence of the platinum center in isomerization kinetics. The cytotoxicity studies in HeLa cell lines allowed to observe that complexes **14** and **15** present better IC_{50} values than that of cisplatin after 24 h of incubation (thus exhibiting faster action than cisplatin), as well as that the influence of the *cis–trans* ligand isomerization in terms of cytotoxicity does not show significant differences. Evaluation of cell uptake revealed a crucial role of the ligands in the internalization of complexes, resulting them to be the key point for the improvement in contrast with cisplatin in some cases.

The interaction of the compounds with DNA, either by direct binding or by intercalation mechanism, confirmed that the *cis–trans* isomerization of the ligands can affect the way in which the complexes interact with DNA but in any case, the intercalating abilities of these complexes are very weak. Finally, the interaction of complexes **14** and **17** with proteins by ESI–MS allows to conclude that the azobenzene ligand plays a crucial role in the survival of complex **14** against the different proteins to which it has been exposed.

In summary, this work aims to contribute to the field of understudied platinum(II) complexes with azobenzene-type ligands and thus provide knowledge about these metal complexes that undoubtedly show great potential in the discovery of new applications in different fields.

Supplementary Information The online version contains supplementary material available at https://doi.org/10.1007/s00775-021-01865-9.

Acknowledgements We acknowledge the Spanish *Ministerio de Ciencia e Innovación* for financial support (projects CTQ2010-15380, CTQ2013-41161-R, and the MINECO-FEDER (BIO2015-67358-C2-2-P and RTI2018-098027-B-C22). We are also members of the *Grup de Recerca de la Generalitat de Catalunya*, ref. 2017SGR-864. K. G. S. acknowledges to the UAB the PIF grant. We also thank the *Servei d'Anàlisi Química* (SAQ) at the *Universitat Autònoma de Barcelona* for allocating instrument time.

Declarations

Conflict of interest The authors declare that there is no known competing financial interests or personal relationships that could have appeared to influence the work reported in this paper.

References

1. Worldwide cancer data. Global cancer statistics for the most common cancers. https://www.wcrf.org/dietandcancer/cancer-trends/worldwide-cancer-data. (Accessed 11 May 2020)
2. Sumit G (2019) Cisplatin: the first metal based anticancer drug. Bioorg Chem 88:102925–102945. https://doi.org/10.1016/j.bioorg.2019.102925
3. Bai L, Gao C, Liu Q, Yu C, Zhang Z, Cai L, Yang B, Qian Y, Yang J, Liao X (2017) Research progress in modern structure of platinum complexes. Eur J Med Chem 140:349–382. https://doi.org/10.1016/j.ejmech.2017-09-034
4. Mjos KD, Orvig C (2014) Metallodrugs in medicinal inorganic chemistry. Chem Rev 114:4540–4563. https://doi.org/10.1021/cr400460s
5. Oun R, Moussa YE, Wheate NJ (2018) The side effects of platinum-based chemotherapy drugs: a review for chemists. Dalton Trans 47:6645–6653. https://doi.org/10.1039/C8DT00838H
6. Marques MPM, Batista de Carvalho ALM, Mamede AP, Dopplapudi A, Rudic S, Tyagi M, Sakai VG, Batista de Carvalho LAE (2020) A new look into the mode of action of metal-based anticancer drugs. Molecules 25:246–265. https://doi.org/10.3390/molecules25020246
7. Johnstone TC, Park GY, Lippard SJ (2014) Understanding and improving platinum anticancer drugs-phenanthriplatin. Anticancer Res 34:471–476
8. Dasari S, Tchounwou PB (2014) Cisplatin in cancer therapy: molecular mechanisms of action. Eur J Pharmacol 7:364–378. https://doi.org/10.1016/j.ejphar.2014.07.025
9. Bonnet S (2018) Why develop photoactivated chemotherapy. Dalton Trans 47:10330–10343. https://doi.org/10.1039/c8dt01585f
10. de Boer-Maggard TR, Mascharak PK (2014) Photoactivatable metal complexes and their use in biology and medicine. In: Storr T (ed) Ligand des med inorg chem. John Wiley and Sons Ltd
11. Zhang Q, Kuang G, He S, Lu H, Cheng Y, Zhou D, Huang Y (2020) Photoactivatable prodrug-backboned polymeric nanoparticles for efficient light-controlled gene delivery and synergistic treatment of platinum-resistant ovarian cancer. Nano Lett 20:3039–3049. https://doi.org/10.1021/acs.nanolett.9b04981
12. Shi H, Imberti C, Sadler PJ (2019) Diazido platinum(IV) complexes for photoactivated anticancer chemotherapy. Inorg Chem Front 6:1623–1638. https://doi.org/10.1039/C9QI00288J
13. Morales K, Samper KG, Pena Q, Hernando J, Lorenzo J, Rodríguez-Diéguez A, Capdevila M, Figueredo M, Palacios O, Bayón P (2018) Squaramide-based Pt(II) complexes as potential oxygen-regulated light-triggered photocages. Inorg Chem 57:15517–15525. https://doi.org/10.1021/acs.inorgchem.8b02854
14. Srivastava P, Singh K, Verma M, Sivakumar S, Patra AK (2018) Photoactive platinum(II) complexes of nonsteroidal anti-inflammatory drug naproxen: Interaction with biological targets, antioxidant activity and cytotoxicity. Eur J Med Chem 144:243–254. https://doi.org/10.1016/j.ejmech.2017.12.025
15. Reessing F, Szymanski W (2017) Beyond photodynamic therapy: light-activated cancer chemotherapy. Curr Med Chem 24:4905–4950. https://doi.org/10.2174/0929867323666160906103223
16. Najjar A, Rajabi N, Karaman R (2017) Recent approaches to platinum(IV) prodrugs: a variety of strategies for enhanced delivery and efficacy. Curr Pharm Des 23:2366–2376. https://doi.org/10.2174/1381612823666170201161037
17. Agent Mitra K, Gautam S, Kondaiah P, Chakravarty AR (2015) The cis-diammineplatinum(II) complex of curcumin: a dual action DNA crosslinking and photochemotherapeutic. Angew Chem Int Ed 54:13989–13993. https://doi.org/10.1002/anie.201507281
18. Biston M-C, Joubert A, Charvet A-M, Balosso J, Foray N (2009) In vitro and in vivo optimization of an anti-glioma modality based on synchrotron X-ray photoactivation of platinated drugs. Radiat Res 172:348–358. https://doi.org/10.1667/RR1650.1
19. Farrer NJ, Salassa L, Sadler PJ (2009) Photoactivated chemotherapy (PACT): the potential of excited-state d-block metals in medicine. Dalton Trans 48:10690–10701. https://doi.org/10.1039/B917753A
20. Fodor L, Ullmann Y, Elman M (2011) Aesthetic applications of intense pulsed light. Springer
21. O'Hagan MP, Ramos-Soriano J, Haldar S, Sheikh S, Morales JC, Mulholland AJ, Galan M (2020) Visible-light photoswitching of

ligand binding mode suggests G-quadruplex DNA as a target for photopharmacology. ChemComm 56:5186–5189. https://doi.org/10.1039/d0cc01581d
22. Bhattacharyya S, Maity M, Chowdhury A, Saha ML, Panja SK, Stang PJ, Mukherjee PS (2020) Coordination-assisted reversible photoswitching of spiropyran-based platinum macrocycles. Inorg Chem 59:2083–2091. https://doi.org/10.1021/acs.inorgchem.9b03572
23. Presa A, Vazquez G, Barrios LA, Roubeau O, Korrodi-Gregorio L, Perez-Tomas R, Gamez P (2018) Photoactivation of the cytotoxic properties of platinum(II) complexes through ligand photoswitch. Inorg Chem 57:4009–4022. https://doi.org/10.1021/acs.inorgchem.8b00146
24. Moustafa ME, McCready MS, Boyle PD, Puddephatt RJ (2017) Photoswitchable and pH responsive organoplatinum(II) complexes with azopyridine ligands. Dalton Trans 46:8405–8414. https://doi.org/10.1039/C7DT01290J
25. Merino E (2011) Synthesis of azobenzenes: the coloured pieces of molecular materials. Chem Soc Rev 40:3835–3853. https://doi.org/10.1039/C0CS00183J
26. Gunnlaugsson T, Leonard JP, Murray NS (2004) Highly selective colorimetric naked-eye cu(ii) detection using an azobenzene chemosensor. Org Lett 6:1557–1560. https://doi.org/10.1021/ol049895l
27. Cardona MA, Makuc D, Szaciłowski K, Plavec J, Magri DC (2017) Water-soluble colorimetric amino[bis(ethanesulfonate)] azobenzene pH indicators: a UV–vis absorption, DFT, and ^{1}H–^{15}N NMR spectroscopy study. ACS Omega 2:6159–6166. https://doi.org/10.1021/acsomega.7b00887
28. Bandara HMD, Burdette SC (2012) Photoisomerization in different classes of azobenzene. Chem Soc Rev 41:1809–1825. https://doi.org/10.1039/C1CS15179G
29. Tamai N, Miyasaka H (2000) Ultrafast dynamics of photochromic systems. Chem Rev 100:1875–1890. https://doi.org/10.1021/cr980816
30. Tong X, Pelletier M, Lasia A, Zhao Y (2008) Fast cis–trans isomerization of an azobenzene derivative in liquids and liquid crystals under a low electric field. Angew Chem Int Ed 47:3596–3599. https://doi.org/10.1002/anie.200705699
31. Pratihar JL, Mandal P, Lin C-H (2019) Synthesis, characterization, structure and redox property of azo-amido and orthometalated azo-imine platinum(II) complexes. Polyhedron 173:114102–114106. https://doi.org/10.1016/j.poly.2019.07.047
32. Samper KG, Marker SC, Bayón P, MacMillan SN, Keresztes I, Palacios O, Wilson JJ (2017) Anticancer activity of hydroxy- and sulfonamide-azobenzene platinum(II) complexes in cisplatin-resistant ovarian cancer cells. J Inorg Biochem 174:102–110. https://doi.org/10.1016/j.jinorgbio.2017.06.003//
33. El-Gendy BE-DM, Ghazvini Zadeh EH, Sotuyo AC, Pillai GG, Katritzky AR (2013) α-Substitution effects on the ease of S→N-acyl transfer in aminothioesters. Chem Biol Drug Des 81:577–582. https://doi.org/10.1111/cbdd.12092
34. Wang Y, Song W, Hu WJ, Lin Q (2009) Fast alkene functionalization in vivo by photoclick chemistry: HOMO lifting of nitrile imine dipoles. Angew Chem Int Ed 48:5330–5333. https://doi.org/10.1002/anie.200901220
35. Shimogaki T, Oshita S, Matsumoto A (2011) Intercalation of mono- and difunctional azobenzenes as photoresponsible guest molecules into poly(muconic acid) host crystals. Macromol Chem Phys 212:1767–1777. https://doi.org/10.1002/macp.201100096
36. Wen G, Zhang D, Huang Y, Zhao R, Zhu L, Shuai Z, Zhu D (2007) New heterocyclic tetrathiafulvalene compounds with an azobenzene moiety: Photomodulation of the electron-donating ability of the tetrathiafulvalene moiety. J Org Chem 72:6247–6250. https://doi.org/10.1021/jo070651e
37. Kim J, Novak BM, Waddon AJ (2004) Liquid crystalline properties of polyguanidines. Macromolecules 37:8286–8292. https://doi.org/10.1021/ma0493527
38. Kreger K, Wolfer P, Audorff H, Kador L, Stingelin-Stutzmann N, Smith P, Schmidt H-W (2010) Stable holographic gratings with small-molecular trisazobenzene derivatives. J Am Chem Soc 132:509–516. https://doi.org/10.1021/ja9091038
39. AD Ryabov, LG Kuzmina, NV Dvortsova, DJ Stufkens, R van Eldik, Bridging of platinacycles by cis-azobenzenes: synthesis and photochemical study (1993) Structure of the twisted inorganic Z-1,1,2,2-tetrasubstituted diazaethene [(Z)-1,2-diphenyldiazaethene)bis[chloro(((dimethylamino)methyl)phenyl-C,N) platinum(II)]. Inorg Chem 32:3166–3174. https://doi.org/10.1021/ic00066a031
40. Schroeder GM, An Y, Cai Z-W, Chen X-T, Clark C, Cornelius LAM, Dai J, Gullo-Brown J, Gupta A, Henley B, Hunt JT, Jeyaseelan R, Kamath A, Kim K, Lippy J, Lombardo LJ, Manne V, Oppenheimer S, Sack JS, Schmidt RJ, Shen G, Stefanski K, Tokarski JS, Trainor GL, Wautlet BS, Wei D, Williams DK, Zhang Y, Zhang Y, Fargnoli J, Borzilleri RM (2009) Discovery of N-(4-(2-Amino-3-chloropyridin-4-yloxy)-3-fluorophenyl)-4-ethoxy-1-(4-fluorophenyl)-2-oxo-1,2-dihydropyridine-3-carboxamide (BMS-777607), a Selective and orally efficacious inhibitor of the met kinase superfamily. J Med Chem 52:1251–1254. https://doi.org/10.1021/jm801586s
41. Zamora A, Pérez SA, Rothemund M, Rodríguez V, Schobert R, Janiak C, Ruiz J (2017) Exploring the Influence of the aromaticity on the anticancer and antivascular activities of organoplatinum(II) complexes. Chem Eur J 23:5614–5625. https://doi.org/10.1002/chem.201700717
42. Albrecht M (2010) Cyclometalation using d-block transition metals: fundamental aspects and recent trends. Chem Rev 110:576–623. https://doi.org/10.1021/cr900279a
43. García-Antón J, Pons J, Solans X, Font-Bardia M, Ros J (2003) Synthesis, characterisation, and X-ray crystal structure of new Ni(II), Pd(II), and Pt(II) complexes of tridentate pyrazole-based ligands with a NOS-Donor Set. Eur J Inorg Chem 12:2992–3000. https://doi.org/10.1002/ejic.200300035
44. García-Antón J, Pons J, Solans X, Font-Bardia M, Ros J (2003) Synthesis of new Pd(II) complexes containing a thioether-pyrazole hemilabile ligand − structural analysis by 1H, 13C NMR spectroscopy and crystal structure of [PdCl(bdtp)]BF4 [bdtp = 1,5-Bis(3,5-dimethyl-1-pyrazolyl)-3-thiapentane]. Eur J Inorg Chem 45:3952–3957. https://doi.org/10.1002/ejic.200300235
45. Vetráková L, Ladányi V, Al Anshori J, Dvořák P, Wirz J, Heger D (2017) The absorption spectrum of cis-azobenzene. Photochem Photobio Sci 16:1749–1756. https://doi.org/10.1039/c7pp00314e
46. Liu X-M, Jin X-Y, Zhang Z-X, Wang J, Bai F-Q (2018) Theoretical study on the reaction mechanism of the thermal cis-trans isomerization of fluorine-substituted azobenzene derivatives. Advances 8:11580–11588. https://doi.org/10.1039/c8ra01132j
47. Amijs CHM, Van Klink GPM, Lutz M, Spek AL, Van Koten G (2005) Functionalized Homoleptic cis- and trans-C, N-orthochelated aminoaryl platinum(II) complexes. Organometallics 24:2944–2958. https://doi.org/10.1021/om050144s
48. Krooglyak EV, Kazankov GM, Kurzeev SA, Polyakov VA, Semenov AN, Ryabov AD (1996) Inorg Chem 35:4804–4806. https://doi.org/10.1021/ic951180u
49. Wehman E, Van Koten G, Knaap CT, Ossor H, Pfeffer M, Spek AL (1988) Inorg Chem 27:4409–4417. https://doi.org/10.1021/ic00297a016
50. Calbo J, Weston CE, White AJP, Rzepa HS, Contreras-García J, Fuchter MJ (2017) Tuning azoheteroarene photoswitch performance through heteroaryl design. J Am Chem Soc 139:1261–1274. https://doi.org/10.1021/jacs.6b11626

51. Serra F, Terentjev EM (2008) Effects of solvent viscosity and polarity on the isomerization of azobenzene. Macromolecules 41:981–986. https://doi.org/10.1021/ma702033e
52. Whitten DG, Wildes PD, Pacifici JG, Irick G (1971) Solvent and substituent on the thermal isomerization of substituted azobenzenes. Flash spectroscopic study. J Am Chem Soc 93:2004–2008. https://doi.org/10.1021/ja00737a027
53. Hall MD, Telma KA, Chang K-E, Lee TD, Madigan JP, Lloyd JR, Goldlust IS, Hoeschele JD, Gottesman MM (2014) Say no to DMSO: Dimethylsulfoxide inactivates cisplatin, carboplatin, and other platinum complexes. Cancer Res 74:3913–3922. https://doi.org/10.1158/0008-5472.CAN-14-0247
54. Shavaleev NM, Adams H, Best J, Edge R, Navaratnam S, Weinstein JA (2006) Deep-Red Luminescence and efficient singlet oxygen generation by cyclometalated platinum(II) complexes with 8-hydroxyquinolines and quinoline-8-thiol. Inorg Chem 45:9410–9415. https://doi.org/10.1021/ic061283k
55. Cameron D, Eisler S (2018) Photoswitchable double bonds: synthetic strategies for tunability and versatility. J Phys Org Chem. https://doi.org/10.1002/poc.3858
56. Pinato O, Musetti C, Sissi C (2014) Pt-based drugs: the spotlight will be on proteins. Metallomics 6:380–395. https://doi.org/10.1039/c3mt00357d
57. Vorlíčková M, Kejnovská I, Bednářová K, Renčiuk D, Kypr J (2012) Circular dichroism spectroscopy of dna: from duplexes to quadruplexes. Chirality 24:691–698. https://doi.org/10.1002/chir.22064
58. Aleksić MM, Kapetanović V (2014) An overview of the optical and electrochemical methods for detection of DNA-drug interactions. Acta Chim Slov 4:61555–61573
59. Macquet JP, Butour JL, A circular dichroism study of DNA platinum complexes (1978) Differentiation between monofunctional, cis-bidentate and trans-bidentate platinum fixation on a series of DNAs. Eur J Biochem 83:375–385. https://doi.org/10.1111/j.1432-1033.1978.tb12103.x
60. Snyder RD, Hendry LB (2005) Toward a greater appreciation of noncovalent chemical/DNA interactions: application of biological and computational approaches. Environ Mol Mutagen 45:100–105. https://doi.org/10.1002/em.20096
61. Pages BJ, Garbutcheon-Singh KB, Aldrich-Wright JR (2017) Platinum intercalators of DNA as anticancer agents. Eur J Inorg Chem 7:1613–1624. https://doi.org/10.1002/ejic.201601204
62. Ruiz J, Rodríguez V, Cutillas N, Samper KG, Capdevila M, Palacios Ò, Espinosa A (2012) Novel C, N-chelate rhodium(III) and iridium(III) antitumor complexes incorporating a lipophilic steroidal conjugate and their interaction with DNA. Dalton Trans 41:12847–12856. https://doi.org/10.1039/C2DT31654D
63. Samper KG, Rodríguez V, Ortega-Carrasco E, Atrián S, Marechal JD, Cutillas N, Zamora A, de Haro C, Capdevila M, Ruiz J, Palacios O (2014) Understanding the interaction of an antitumoral platinum(II) 7-azaindolate complex with proteins and DNA. Biometals 27:1159–1177. https://doi.org/10.1007/s10534-014-9780-1